


A dual-activity topoisomerase complex promotes both transcriptional activation and repression in response to starvation

Shuaikun Su, Yutong Xue, Seung Kyu Lee, Yongqing Zhang, Jinshui Fan, Supriyo De, Alexei Sharov and Weidong Wang *

Laboratory of Genetics and Genomics, National Institute on Aging, Intramural Research Program, National Institutes of Health, Baltimore, MD 21224, USA

Received October 13, 2022; Revised January 27, 2023; Editorial Decision January 31, 2023; Accepted January 31, 2023

ABSTRACT

Topoisomerases are required to release topological stress generated by RNA polymerase II (RNAPII) during transcription. Here, we show that in response to starvation, the complex of topoisomerase 3b (TOP3B) and TDRD3 can enhance not only transcriptional activation, but also repression, which mimics other topoisomerases that can also alter transcription in both directions. The genes enhanced by TOP3B–TDRD3 are enriched with long and highly-expressed ones, which are also preferentially stimulated by other topoisomerases, suggesting that different topoisomerases may recognize their targets through a similar mechanism. Specifically, human HCT116 cells individually inactivated for TOP3B, TDRD3 or TOP3B topoisomerase activity, exhibit similarly disrupted transcription for both starvation-activated genes (SAGs) and starvation-repressed genes (SRGs). Responding to starvation, both TOP3B–TDRD3 and the elongating form of RNAPII exhibit concomitantly increased binding to TOP3B-dependent SAGs, at binding sites that overlap. Notably, TOP3B inactivation decreases the binding of elongating RNAPII to TOP3B-dependent SAGs while increased it to SRGs. Furthermore, TOP3B-ablated cells display reduced transcription of several autophagy-associated genes and autophagy *per se*. Our data suggest that TOP3B–TDRD3 can promote both transcriptional activation and repression by regulating RNAPII distribution. In addition, the findings that it can facilitate autophagy may account for the shortened lifespan of *Top3b-KO* mice.

INTRODUCTION

Topoisomerases are critical for DNA replication and transcription by relieving topological stress produced by DNA or RNA polymerases (1). Recently, human TOP3B (a Type IA topoisomerase) has attracted increasing attention because it was found to be a dual-activity topoisomerase that can change the topology for RNA as well as DNA (2). Subsequent studies indicated that this DNA/RNA dual-activity is prevalent in Type IA topoisomerases from all three domains of life (bacteria, archaea, and eukaryotes) (3,4). This has led to the hypothesis that TOP3B and other dual activity topoisomerases may resolve topological problems produced during both DNA and RNA-based cellular processes (2,4,5). The hypothesis is supported by several lines of evidence. For DNA, TOP3B has been shown to stimulate neuronal activity-dependent transcription in mouse brains (6), and to resolve R-loops formed during transcription both *in vitro* and in cells (7,8). For RNA, TOP3B can directly bind mRNAs, associate with polyribosomes and RNA-stress granules (2,3), regulate mRNA translation and turnover (9); and promote replication of positive-strand RNA viruses including SARS-CoV-2 (10). Moreover, an over-expression of a TOP3B mutant protein can generate intermediates of topoisomerase reactions (cleavage complexes) on both DNA and RNA in human cell lines (11).

TOP3B forms a conserved complex with TDRD3 (Tudor domain-containing 3) in both human and *Drosophila* (2,8,12). TDRD3 can act as a regulatory subunit to enhance the binding and topoisomerase activity of TOP3B on both DNA and RNA *in vitro* (2,4,13). In addition, TDRD3 tethers TOP3B to other proteins through several protein-binding motifs, including a Tudor domain that recognizes methylated arginine residues (2,8,14–16). The TDRD3-interacting proteins include those that can act on DNA, such as RNA polymerase II (RNAPII) (15); and those on mRNA, including Fragile-X mental retardation protein (FMRP) and RNA-induced silencing

*To whom correspondence should be addressed. Tel: +1 410 454 8418; Email: wangw@grc.nia.nih.gov

complex (2,14,17). These data suggest that the two proteins may act as a complex (termed TOP3B–TDRD3) to coordinately solve topological problems on both DNA and RNA. This notion is supported by evidence that the TOP3B and TDRD3 can function in the same cellular processes on DNA or RNA, which include: neuronal activity-dependent transcription (6), R-loop resolution (8) and mRNA translation and turnover (9).

In response to starvation, cells can obtain nutrients through autophagy, which is a lysosomal-mediated process of cytoplasmic degradation of organelles, protein aggregates and pathogens. Autophagy is essential for stress survival and normal lifespan of organisms (18,19). Normal induction of autophagy by starvation depends on transcriptional activation of many autophagy-associated genes (20). However, whether this transcriptional activation requires topoisomerases remain unclear. Notably, *Top3b-KO* mice display shortened lifespan (21), raising a possibility that transcriptional activation of autophagy genes may be defective in the absence of TOP3B.

This study aims to address three unanswered questions regarding how TOP3B–TDRD3 functions in transcription. First, can TOP3B–TDRD3 regulate starvation-induced transcription? Second, does TOP3B–TDRD3 and its topoisomerase activity act coordinately to promote transcription? Third, does TOP3B–TDRD3 play a role in regulating autophagy? We have recently established a non-neuronal human HCT116 cell system (derived from colon cancer) in which we individually inactivated TOP3B, TDRD3 and the TOP3B topoisomerase activity (Y336F) (9). We used these cells to show that TOP3B and TDRD3 coordinately regulate mRNA translation and turnover, in both topoisomerase activity-dependent and independent manners. Here we used the same cells to show that TOP3B–TDRD3 and its topoisomerase activity coordinately regulate starvation-induced transcription. Notably, TOP3B–TDRD3 promotes not only transcriptional activation, but also repression. Moreover, *TOP3B-KO* cells show reduced expression of several autophagy genes, and these cells and *Top3β* mutant *Drosophila* exhibit reduced autophagy. Since autophagy plays a critical role in aging (22), defective transcription of starvation-induced autophagy genes could be a mechanism that contributes to the shortened lifespan observed in *Top3b-KO* mice.

MATERIALS AND METHODS

Cell lines and cell starvation treatment

HCT116 cells were cultured in Dulbeccos' modified Eagle's medium (DMEM, Thermo Fisher Scientific) supplemented with 10% fetal bovine serum (HyClone) and 1% antibiotics (Penicillin-Streptomycin, Sigma). The generation of the *TOP3B-KO1*, *TOP3B-KO2*, *TDRD3-KO1*, *FMRI-KO* and *Y336F-KI* HCT116 cell lines by CRISPR-Cas9 were as described previously (9). *TDRD3-KO2* cells were generated using the same protocol, and its sgRNA sequence and immunoblotting confirmation were shown in Supplementary Figure S1A, B. For generation of the *TOP3B-KO1* HCT116 cell lines with stably-expressed TOP3B or TOP3B-Y336F protein, we used the retrovirus vector system (adgene, pBABE-puro #1764, pUMVC #8449 and pCMV-

VSV-G #8454). First, we cloned each gene without any tags into the pBABE-puro plasmid. Then the retroviruses carrying the transgenes were generated from HEK293 cells, and were used to infect *TOP3B-KO1* HCT116 cells for 2 days. Subsequently, the cells were selected by culturing in medium containing 1 μg/ml puromycin for 7 days. The puromycin-resistant cells were collected. Western blot was used to detect the expression of TOP3B or TOP3B-Y336F protein. For cell starvation, HCT116 cells were seeded at a concentration that will enable them to reach 60%–80% confluency in 12–16 h. Cell culture medium was removed. Then warm (37°C) Phosphate-Buffered Saline (PBS, pH 7.4, 10010023, Gibco™) was used to wash the cells once. Warm (37°C) Earle's Balanced Salt Solution (EBSS, CaCl₂ 0.20 g/l, KCl 0.40 g/l, MgSO₄ 0.097 g/l, NaCl 6.80 g/l, NaHCO₃ 2.20 g/l, NaH₂PO₄–H₂O 0.14 g/l, Glucose 1.00 g/l, Phenol Red 0.01g/l) (24010043, Gibco™) was added, and the cells were incubated at 37°C CO₂ cell culture incubator for 6 h before collection.

RNA extraction and RT-qPCR

HCT116 cells were cultured in 24-well plates for 12–16 h. Then different treatments were performed as described above or in the main text. RNA was extracted by TRIzol (Invitrogen, 15596026) following the instruction. The cDNA was synthesized from 1 μg RNA using Taqman Reverse Transcription Reagents (Applied Biosystems, N8080234). After 5–10-fold dilution, the cDNA was used as a template to perform qPCR with SYBR Green PCR Master Mix (Applied Biosystems, 4309155). The PCR primer sequences are shown in Supplementary Table S10.

LysoTracker staining

WT and *TOP3B-KO* HCT116 cells were treated with EBSS for 3 or 6 h. Then 1 μM LysoTracker (Invitrogen, L7528) was added into the medium for 15–20 min before fixing and then images were captured under confocal microscope. LysoTracker staining density was measured by ImageJ. *Drosophila* stocks were maintained as previously described (14). The wandering third instar larvae were transferred to a 6 cm petri dish with two layers of filter papers that were coated with yeast paste (no treatment) or water (starved). The larvae were kept at 25°C for 6 h, followed by a brief rinsing with PBS. The treated larvae were immediately dissected to isolate the fat bodies. The fat bodies were incubated with LysoTracker Red (1:5000) for 10 min at room temperature, followed by washing twice with PBS (5 min each). Then the samples were fixated in 4% paraformaldehyde (PFA) for 20 min and washed 3 times. The samples were mounted in the ProLong Gold Antifade Reagent with DAPI (Invitrogen). The samples were imaged with Zeiss LSM-880 confocal laser scanning microscopy. For quantification of the LysoTracker positive signals, respective channels were separated. The intensity and particle number per area/cell was measured using ImageJ.

Western blot

For the western blot of LC3 protein, HCT116 cells were cultured for 16–20 h, then starved by replacing medium with

EBSS for 2–6 h. Cells were washed twice in ice-cold PBS with protease and phosphatase inhibitors before harvesting by scraping with a plastic cell remover. Cells were pelleted by centrifugation at $4000 \times g$ for 3 min at 4°C and then lysed for 15 min on ice (vortexed every 5 min) in two volumes of RIPA buffer. Total 60 μg of protein were separated on a 4–15% SDS-PAGE gel. After electrophoresis, proteins were transferred to a 0.45- μm nitrocellulose membrane. The membrane was cut at 26 kDa to avoid cross-reaction of the primary antibody with nonspecific bands at higher molecular weights. The membrane was then blocked for 1 h at room temperature in 5% milk (in PBS). The portion of the membrane below 26 kDa was probed with a primary antibody against to LC3 (Novus, cat # NB600-1384, 1:2000) overnight at 4°C . The portion of the membrane above 26 kDa was probed with anti-ACTB antibody as a control for gel loading. No Tween-20 was added to the primary antibody incubation solution (5% milk in PBS), but 0.05% Tween-20 was used to wash the membranes (three times) after the primary and secondary antibody incubations. The membranes were incubated with anti-rabbit secondary antibody (1:5000) for 2 h at room temperature, then washed three times with 0.05% Tween-20 in PBS. Detection was performed by enhanced chemiluminescence. For Western blot of TOP3B protein, an anti-TOP3B antibody (Sigma, cat# WH0008940M1-100UG, 1:1000) was used. Tween-20 was added to the primary antibody incubation solution. Other steps were similar with those above.

RNA-seq

The mRNAs were purified from 10 μg total RNA using oligo dT beads (61012, Invitrogen). The purified mRNAs were used for RNA-seq library preparation by following a published protocol (6).

ChIP-seq

ChIP-seq was performed as previously described (6,9). One 15 cm plate of HCT116 cells cultured in 20 ml DMEM containing 10% FBS was crosslinked with 0.54 ml of 37% formaldehyde (final concentration is 1%) at 37°C for 15 min. For starvation groups, DMEM was removed, and the cells were washed one time using 5 ml PBS. Then the cells were incubated in 20 ml EBSS medium for 6 h before crosslinking. The crosslinking reaction was terminated by removing the medium. The cells were washed once with 10 ml of $1 \times$ PBS, and then the buffer was removed leaving 0.5 ml in the plate. Cells were harvested by scraping and concentrated by centrifugation at 3000 rpm at 4°C for 2 min. The cell pellet was resuspended in 5 volumes of RIPA buffer (150 mM NaCl, 20 mM Tris pH 7.5, 2 mM EDTA, 1% NP40, 0.5% Na-Deoxycholate acid, 0.1% SDS) containing 1mM PMSF and $1 \times$ protease inhibitor cocktail. The resuspended cells were sonicated in ice-cold water bath with the Diagenode Bioruptor Sonication System to break chromatin to about 0.3–1 kb. The setting of the Bioruptor is for 4×5 min with 15 s ON and 15 seconds OFF cycles at high power setting. After sonication, the cells were centrifuged in a 4°C microfuge at 14 000 rpm for 10 min. The supernatant containing soluble chromatin fraction is saved for ChIP.

The above chromatin fraction was precleared by incubation with 100 μl of protein A beads for 1 h at room temperature. The ChIP mixture contains 500 μl of the precleared chromatin fraction, 2.5 μl of 20 mg/ml BSA, 30 μl of the protein A beads, and the indicated amounts of antibodies. The antibodies include: 2 μg of anti-RNA polymerase II CTD CL8WG16 (Sigma, Cat#: 05-952-I), RNAPII-ser2p antibody (abcam, ab5095), 5 μg of TDRD3 (D3O2G) antibody (Cell Signaling Technology, Cat#: 5942). The mixture was incubated at 4°C overnight with rotation. The beads were collected by centrifugation using a microfuge for 1 min at 3000 rpm at 4°C . They were washed twice with RIPA buffer supplemented with 0.3M NaCl, twice with RIPA buffer supplemented with 0.15 M NaCl, twice with LiCl buffer ($1 \times$ TE, 0.25M LiCl, 0.5% NP-40, 0.5% Na-Deoxycholate), and twice with $1 \times$ TE buffer (Tris-HCl, pH 8.0, 10 mM; EDTA, 1 mM). The beads were resuspended in 100 μl of $1 \times$ TE buffer. 2.5 μl of 10% SDS, 5 μl of 10 mg/ml Proteinase K were then added and incubated at 65°C overnight to release DNA from the bound proteins and beads. About 100 μl of chromatin fraction was saved as the ‘input’ which was also treated with SDS and proteinase K. The supernatant was collected by centrifugation. The remaining beads were eluted one more time with 100 μl of $1 \times$ TE. The eluted supernatants were combined and extracted twice with 1 volume of Phenol/Chloroform to remove proteins. The DNA from aqueous fraction containing was precipitated with 1 μl of 20 mg/ml glycoblue, 20 μl of 3M NaOAc (pH 5.2) and 500 μl of 100% ethanol followed by incubation for 10 min on dry ice. The precipitated DNA was collected by centrifugation for 20 min at 4°C in a microfuge. The DNA pellet was washed once with 75% ethanol, air dried, and resuspended in 40 μl of $1 \times$ TE. The DNA was then used for library preparation and sequencing. Library preparation was described in a previous publication (6).

Bioinformatics analysis

RNA-seq data analysis was as described (9). Briefly, the reads of RNA-seq were mapped to human genome (hg38) with HISAT2 (23). The raw read counts were generated by HTSeq-Count (24). The genes with total counts (untreated and treated groups) less than 10 were removed. Differentially expressed genes (DEGs) in RNA-seq were identified by DESeq2 (25). The DEGs between no treatment group and starvation group were identified by implementing a threshold of fold change >2.0 , adjusted P -value <0.05 . The threshold of fold change >1.5 and adjusted P -value <0.1 was used for the DEGs of *TOP3B-KO*, *TDRD3-KO* and *Y336F-KI* cells. Heatmaps of RNA-seq were drawn by pheatmap (RRID:SCR_016418) using row-normalized z-scores or by Excel using fold changes. The volcano plots were drawn in Excel using fold changes and adjusted P -values generated by DESeq2. The randomly selected control genes used in Figure 1G, Figure 2E, Supplementary Figure S3, Figure S4C, Figure S4F and Figure S5 were both gene number and expression level matched. To match the expression level of the DEGs, first, we divided the expressed genes into three groups based on their RNA levels in no treatment *WT* cells: high (top 33%), medium

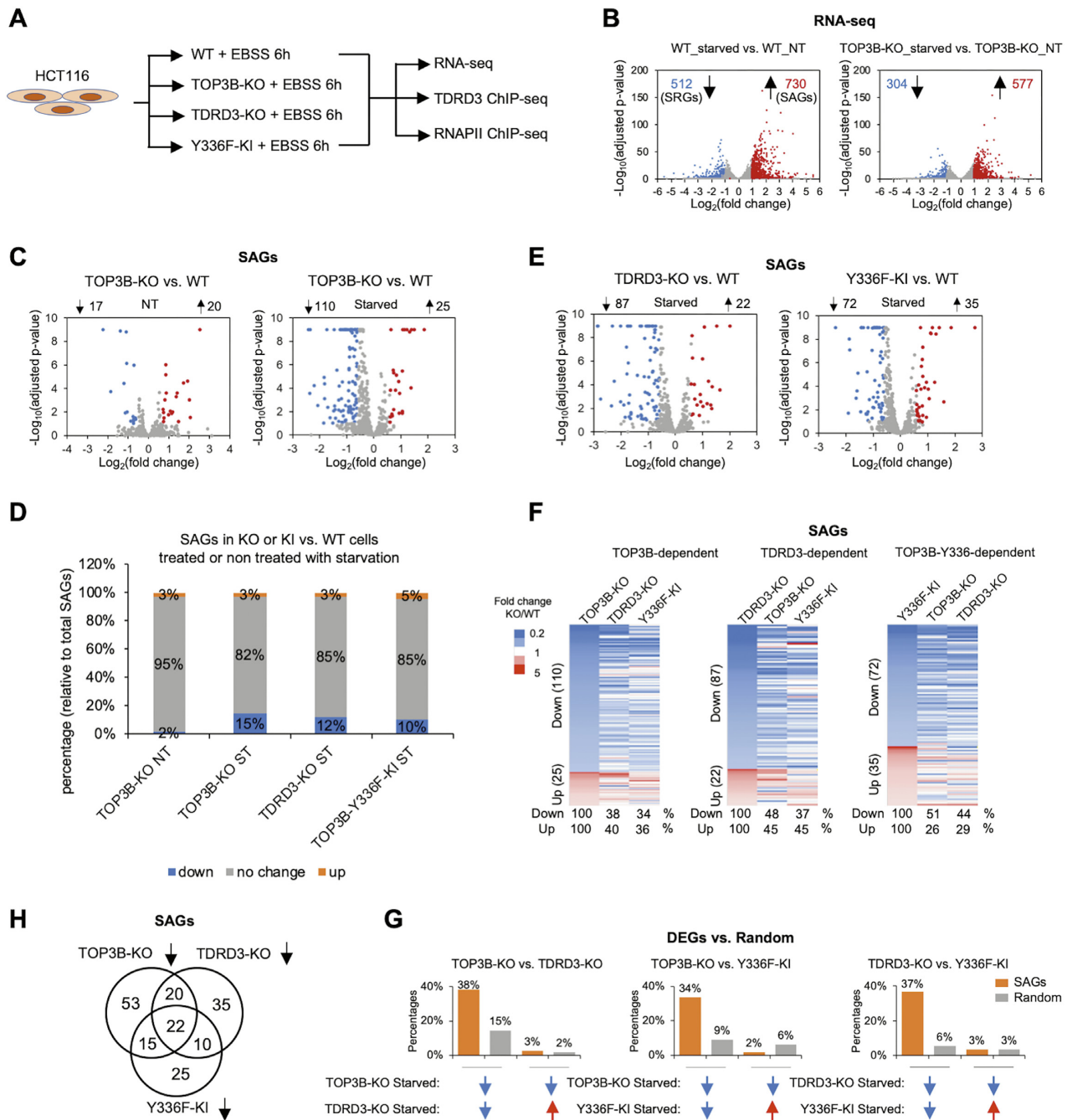


Figure 1. TOP3B–TDRD3 and its topoisomerase activity promote starvation-activated transcription. (A) A schematic diagram showing the experimental design procedure. (B) Two volcano plots showing the genes differentially expressed (fold change > 2 and adjusted *P*-value < 0.05) in *WT* (left) or *TOP3B-KO* (right) cells starved for 6 h (starve) compared with no treatment (NT) cells were identified using DESeq2. The numbers of the genes significantly up- or down-regulated in starved cells are indicated. SAGs, starvation-activated genes; SRGs, starvation-repressed genes. (C) Expression level changes of SAGs between *TOP3B-KO* and *WT* cells under no treatment (left) or starvation condition (right). The significantly reduced or increased genes (fold change > 1.5 and adjusted *P*-value < 0.1) were marked in blue or red color separately. (D) The bar graph showing the expression level changes of the SAGs vs *WT* in *TOP3B-KO* cells under nontreatment condition, or in *TOP3B-KO*, *TDRD3-KO*, *TOP3B-Y336F-KI* cells under starvation condition. The percentages were calculated by dividing the number of total SAGs (*n*=730). (E) Expression level changes of SAGs between *TDRD3-KO* and *WT* cells (left) or *Y336F-KI* and *WT* cells (right) under starvation condition. (F) Three heatmaps showing the expression level changes of the TOP3B-dependent, TDRD3-dependent, TOP3B-Y336 dependent SAGs between *WT* and *TOP3B-KO*, *WT* and *TDRD3-KO*, *WT* and *TOP3B-Y336F-KI* cells under starvation condition. Blue color represents decreased genes and red color represents increased genes in the mutant cells. The table below shows the percentages of genes altered in the same directions in different mutant cells. (G) Bar graphs showing the percentages of overlapping genes altered in the same or opposite directions between the TOP3B-dependent, TDRD3-dependent and TOP3B-Y336-dependent SAGs (orange). The percentages of overlapping genes between the three mutant dependent SAGs and the randomly selected genes separately (expression levels and gene numbers matched to the three mutant dependent SAGs) were shown as controls (grey). Blue arrows represent reduced, whereas red arrows represent increased DEGs. (H) Venn diagram showing the overlapped gene numbers between the reduced SAGs in three different mutant cells. The RNA-seq data used to analyze were from three different biological replicates.

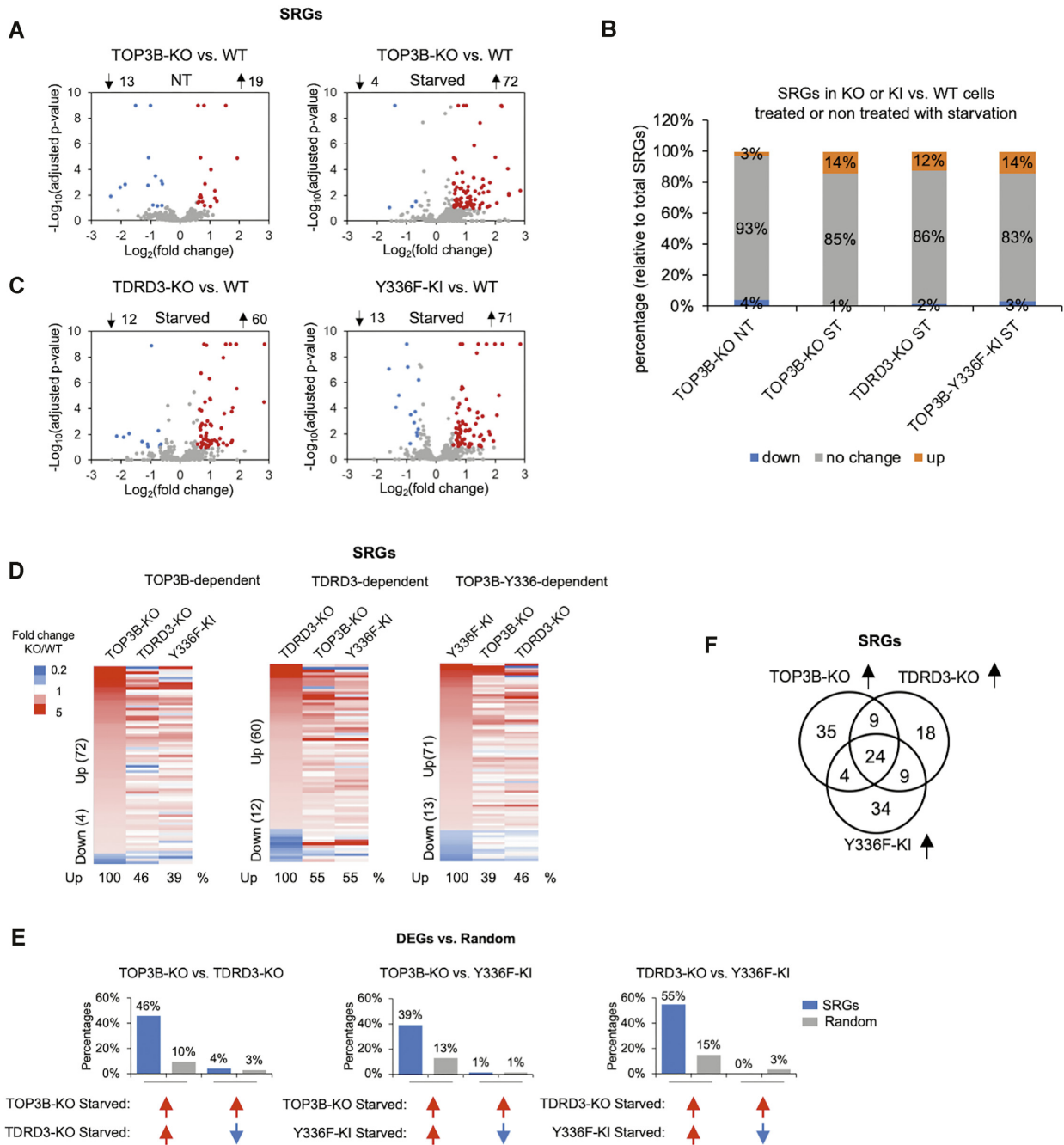


Figure 2. TOP3B–TDRD3 and its topoisomerase activity suppress starvation-repressed transcription. (A) Expression level changes of the starvation-repressed genes (SRGs) between *TOP3B-KO* and *WT* cells under no treatment (left) or starvation condition (right). The significantly reduced or increased genes (fold change > 1.5 and adjusted *P*-value < 0.1) are marked in blue or red color separately. (B) The bar graph showing the expression level changes of the SRGs vs *WT* in *TOP3B-KO* cells under nontreatment condition, or in *TOP3B-KO*, *TDRD3-KO*, *TOP3B-Y336F-KI* cells under starvation condition. The percentages were calculated by dividing the number of total SRGs (n=512). (C) Expression level changes of the SRGs between *TDRD3-KO* and *WT* cells (left) or *Y336F-KI* and *WT* cells (right) under starvation condition. (D) Three heatmaps showing the expression level changes of the TOP3B-dependent, TDRD3-dependent, TOP3B-Y336F-KI dependent SRGs between *WT* and *TOP3B-KO*, *WT* and *TDRD3-KO*, *WT* and *TOP3B-Y336F-KI* cells under starvation condition. Blue color represents decreased genes and red color represents increased genes in the mutant cells. The table below shows the percentages of SRGs increased in different mutant cells. (E) Bar graphs showing the percentages of overlapping genes altered in the same or opposite directions between the TOP3B-dependent, TDRD3-dependent and TOP3B-Y336F-KI dependent SRGs (blue). The percentages of overlapping genes between the three mutants dependent SRGs and the randomly selected genes separately (expression levels and gene numbers matched to the three mutants dependent SRGs) were shown as controls (grey). Blue arrows represent reduced, whereas red arrows represent increased DEGs. (F) Venn diagram showing the overlapped gene numbers between the increased SRGs in three different mutant cells. The RNA-seq data used to analyze were from three different biological replicates.

(middle 33%) and low (bottom 33%). Then, we identified the number distributions of the DEGs in the three groups. Finally, randomly selected the same number control genes from the three groups using R function were used to compare. The randomly selected genes used in expression level comparison (Supplementary Figure S4E) were gene number matched. ChIP-seq reads were mapped to human genome (hg38) with Bowtie2 allowing maximum of two mismatches (26). BAM format files were generated from SAM format files using Samtools (27). The bigwig format files, heatmaps, profile plots were generated by deepTools (28). For RNAPII and RNAPII-ser2p ChIP-seq normalized read counts near transcription start site (TSS) regions (−500 to +500 bp) and transcription end site (TES) regions (0 to −2000 bp) were generated by BEDTools (29). For TDRD3 binding peak analysis, we called peaks by MACS2 (30) using input as a control (fold change > 1.5, *q*-value < 0.05). Only the peaks identified by both replicates (*WT* groups) were used to extract reads counts by BEDTools. The normalized read counts from peak regions were used to calculate the fold changes in Excel. The enriched peaks (Fold change (WT/KO) > 1.5 in both replicates) were selected and annotated using HOMER (31).

Statistical analysis

For RNA-seq and ChIP-seq analysis, adjusted *p*-values were generated by DESeq2. The differentially expressed genes (DEGs) caused by starvation were identified by DESeq2 using the threshold (adjusted *p*-value < 0.05 and fold change > 2.0). The DEGs between *WT* and mutant cells were identified by the threshold (adjusted *p*-value < 0.1 and fold change > 1.5). For the bar graphs generated using normalized read counts of RNA-seq, *P*-values generated from DESeq2 were used to label the significance. For the RNAPII-ser2p level differences of TOP3B-dependent SAGs or SRGs, the averages of RNAPII-ser2p normalized read counts at TES region were used to generate the bar graphs. Student *t*-test was used to show the significant differences between two groups. For the RT-qPCR results, western blot gel density, LysoTracker density differences, student *t*-test was used to calculate the significant differences between two groups. For RNA-seq and RNAPII-ser2p/RNAPII ChIP-seq, three biological replicates were performed. For TDRD3 ChIP-seq, two biological replicates were performed. For RT-qPCR, western blot and LysoTracker staining results, three biological replicates were performed. All the bar graphs were generated by Excel or GraphPad Prism.

For experiments of more than two groups, we also used ANOVA test (Prism 8) to calculate the significant differences between samples, and showed the results in Supplementary Figure S8.

RESULTS

TOP3B enhances transcriptional activation of a subset of genes in response to starvation

We used the isogenic HCT116 cell lines of *TOP3B-knockout* (*KO*), *TDRD3-KO* and a *TOP3B-Y336F-knockin* (*Y336F-KI*) mutant to examine the roles of TOP3B–TDRD3 in

genome-wide transcription by employing a strategy used previously to demonstrate the importance of the complex in neuronal activity-dependent transcription (Figure 1A) (6). Specifically, we performed RNA-seq and RNAPII ChIP-seq to identify transcriptome changes in the mutant vs. *WT* cells; and then used TDRD3 ChIP-seq to identify the genes that are directly bound by the complex. We also focused on studying whether TOP3B–TDRD3 is important for transcription when cells are under stress, based on our earlier findings that Top3b regulates fewer genes under basal than neuronal activity-activated condition (6). After testing several stresses (starvation, arsenic stress, proinflammatory cytokine treatment, and DNA damage), we found that starvation-activated transcription has the strongest dependence on TOP3B–TDRD3 and will describe our findings below.

We cultured the cells under starvation of both serum and nutrients, by growing them in EBSS (Earle's Balanced Salt Solution), which is free of serum and a key nutrient: amino acids. This starvation method has been widely used to starve cells and induce autophagy (20). Our RNA-seq analysis revealed that starvation of *WT* HCT116 cells increased the RNA levels of 730 genes (named as SAGs for Starvation-Activated Genes), whereas repressed those of 512 genes (named SRGs for Starvation-Repressed Genes) (fold change > 2 and adjusted *P*-value < 0.05) (Figure 1B, left and Supplementary Table S1). Subsequent elongating RNAPII (RNAPII-ser2p) ChIP-seq analysis showed that these RNA level changes elicited by either starvation or TOP3B inactivation mainly occur at the transcriptional levels (Supplemental Results, Figure S2A–B). KEGG pathway analysis revealed that autophagy is among the top pathways enriched in the SAGs (Supplementary Figure S2C), whereas metabolism is among top pathways in SRGs (Supplementary Figure S2D). These data are largely consistent with previous findings that starvation can induce gene expression at the transcription level (20). Interestingly, the numbers of total SAGs and SRGs identified by RNA-seq in starvation-treated *TOP3B-KO* cells (abbreviated as *TOP3B-KO-ST*) (577 and 304, respectively; Supplementary Table S2) were about 40% and 21%, respectively, fewer than those in *WT-ST* (starvation-treated) cells (Figure 1B, right versus left), implying that TOP3B is needed to promote both transcriptional activation and repression in response to starvation.

Volcano plot analysis of the 730 SAGs revealed that nontreated (grow cells in normal medium) *TOP3B-KO* cells (abbreviated as *TOP3B-KO-NT*) displayed significantly altered RNA-seq levels of only 37 SAGs (fold change > 1.5, adjusted *P*-value < 0.1), with the numbers of decreased and increased genes similar to each other (17 versus 20; <1.5-fold difference) (Figure 1C, left and Figure 1D). Under starvation, *TOP3B-KO* cells showed about 4 times more significantly altered SAGs than under nontreated condition (135 versus 37) (Figure 1C, Figure 1D and Supplementary Table S3), consistent with our earlier data (6) that TOP3B is more important for activated than basal transcription. The number of reduced SAGs (110 or 15% of total SAGs) in *TOP3B-KO-ST* cells is about 4.6 times more than those of the increased (25 or 3%) (Figure 1C and D). Moreover, the SAGs decreased in *TOP3B-KO-ST* cells under starvation (*n*=110) were about 6 times more those under nontreatment

conditions ($n=17$), whereas the SAGs increased in the *KO-ST* cells were not drastically altered vs. those of *KO-NT* cells (Figure 1C and D). These data suggest that TOP3B enhances transcription of SAGs mainly under starvation.

We noted that fewer than 20% of total SAGs are significantly altered (fold change > 1.5 and adjusted P -value < 0.1) in *TOP3B-KO-ST* cells, and named these genes as TOP3B-dependent SAGs (Figure 1D). In contrast, the majority (80%) of SAGs remain unaltered (Figure 1D). The data indicate that TOP3B regulates only a small fraction of SAGs, and other topoisomerases may regulate the remaining SAGs (Su et al., manuscript in preparation).

TDRD3 and TOP3B-topoisomerase activity preferentially enhance starvation-activated transcription

We then analyzed *TDRD3-KO* and *TOP3B-Y336F-KI* HCT116 cells by RNA-seq to study whether the entire TOP3B–TDRD3 complex and its topoisomerase activity can coordinately regulate starvation-induced transcription. RNA-seq data showed that both *TDRD3-KO* and *TOP3B-Y336F-KI* cells have similar numbers or percentages of differentially expressed SAGs (109 and 107, respectively) (Figure 1D–E, and Supplementary Tables S4–S6) when compared to *TOP3B-KO* cells (135) (Figure 1C, right). In addition, the numbers or percentages of decreased SAGs in *TDRD3-KO* and *TOP3B-Y336F-KI* cells are 2–4-fold more than those of increased SAGs (Figure 1D, E), which resemble the difference in *TOP3B-KO* cells (~4-fold in the same comparison). Furthermore, the observed percentages of decreased SAGs among different mutant cells occurred at much higher frequency than those of the same numbers of randomly selected and expression level-matched genes (random controls) (Supplemental Results; Figure S3A). These data suggest that the entire TOP3B–TDRD3 complex and its topoisomerase activity preferentially enhance transcription of SAGs.

To further compare the effects of the three mutant cells on SAGs, we made 3 separate heatmaps to assess whether the SAGs that are significantly decreased or increases in each mutant cell line exhibit the same patterns of alteration in the other two mutant lines (Figure 1F). The patterns of the three heatmaps were strikingly similar. For example, all mutant lines showed more decreased than increased SAGs (2–5-fold) (Figure 1F, more blue than red colors). Moreover, the SAGs significantly decreased in one mutant line had a strong preference to be decreased in the other two lines (Figure 1F, see co-clustering of blue color), whereas the SAGs increased in one mutant line also had a tendency to be increased in other two mutants (Figure 1F, see co-clustering of red color). The data suggest that TOP3B, TDRD3 and the TOP3B topoisomerase activity have strong preference to act coordinately in regulating transcription of SAGs.

We specifically calculated whether the SAGs that are significantly decreased in one mutant cell line preferentially exhibit the same direction of alteration (decrease) in the other two mutant lines. For the 110 SAGs that show significant decrease in *TOP3B-KO-ST* cells, 38% and 34% of them showed the same direction of alteration in *TDRD3-KO-ST* and *TOP3B-Y336F-ST* cells, respectively; whereas merely 3% and 2% of them displayed the opposite direc-

tion of alteration (increase), respectively (Figure 1G, left and middle, lane 1 versus 3). Similarly, For the 87 SAGs that show significant decrease in *TDRD3-KO-ST* cells, 37% showed the same direction of alteration, whereas merely 3% exhibited the opposite direction of alteration, in *TOP3B-Y336F-ST* cells (Figure 1G, right, lane 1 versus 3). Thus, in each pair of mutant lines, the percentages of SAGs altered in the same directions are 12–20-fold higher than those altered in the opposite directions, suggesting that the entire TOP3B–TDRD3 complex and its topoisomerase activity coordinately enhance transcription of SAGs.

We assessed if the observed SAGs showing the same or opposite directions of alterations between each pair of mutant cell lines could happen by chance. We found that for SAGs showing significant decrease in *TOP3B-KO-ST* or *TDRD3-KO-ST* cells, the observed percentages of genes showing the same direction of alteration in other mutant cells were more than 2–6-fold higher than those of random controls (Figure 1G, lanes 1 versus 2, in each graph). In contrast, the observed percentages of SAGs showing the opposite directions of alteration were similar or lower than those of random controls (Figure 1G, lanes 3 versus 4). The analysis supports the notion that TOP3B–TDRD3 and the topoisomerase activity coordinately stimulates transcription.

Venn diagram analysis identified 22 SAGs decreased in all three mutant lines (Figure 1H). This number is larger than those decreased in two but not three mutant cells ($n=20, n=15, n=10$). This difference was also observed for SRGs that are increased in all three mutant lines (see Figure 2F). The data support the notion the entire TOP3B–TDRD3 complex and their topoisomerase activity preferentially work together to regulate starvation-induced transcription.

Venn diagram also identified 53 SAGs decreased in only *TOP3B-KO*, but not *TDRD3-KO* and *TOP3B-Y336F-KI* mutant cells (Figure 1H), suggesting that TOP3B can regulate transcription of some genes independent of TDRD3 or its topoisomerase activity (Figure 1H). It also identified 35 SAGs that are only decreased in *TDRD3-KO*, but not in other two mutant cells, suggesting that TDRD3 may regulate transcription of some genes independent of TOP3B. Moreover, it identified 25 SAGs that are decreased in only *TOP3B-Y336F-KI* cells, but not *TOP3B-KO* or *TDRD3-KO* cells. It is possible that the last group of decreased SAGs are caused by gain-of-function activity of *TOP3B-Y336F-KI* mutant (9).

TOP3B–TDRD3 and its topoisomerase activity promote starvation-repressed transcription

We next studied whether TOP3B–TDRD3 and its topoisomerase activity can coordinately promote starvation-repressed transcription, by analyzing the decreased or increased SRGs in the same three mutant cells by the same methods as above. The volcano plots and heatmaps obtained for SRGs were similar to those of SAGs (Figure 2 versus Figure 1), except that the main effect of TOP3B–TDRD3 inactivation on SRGs is to increase their transcription, which is opposite of its effect on SAGs.

First, plots made in parallel to those of Figure 1C–H revealed that only 32 of 512 SRGs (6%) were significantly

altered in *TOP3B-KO-NT* cells, and the numbers of the decreased and increased genes were comparable (13 versus 19; <1.5-fold difference) (Figure 2A, left and Figure 2B). In contrast, about 2.5-fold more SRGs (76 or 15%) were significantly altered in *TOP3B-KO-ST* cells, and the numbers of the increased versus decreased SRGs are 72 versus 4, an 18-fold difference (Figure 2A, right and Figure 2B). Moreover, the number of increased SRGs under starvation ($n=72$) was about 4 times more than that without treatment ($n=19$), whereas the number of the decreased SRGs was about 3 times fewer (4 versus 13) (Figure 2A, right versus left; Figure 2B). These results resemble those of the altered SAGs in *TOP3B-KO-ST* cells (Figure 1C–E), and suggest that while TOP3B has a small effect on either SAGs or SRGs under nontreatment condition, it has a strong effect under starvation—enhancing both repression of SRGs and activation of SAGs.

Second, the plots made in parallel to those in Figure 1D and 1E revealed that the numbers or percentages of the increased SRGs in *TDRD3-KO* and *TOP3B-Y336F* cells were about 5-times more than those of the decreased SRGs (Figure 2B, C), which mimics the 18-fold difference in *TOP3B-KO* cells. Moreover, the observed percentages of increased SRGs among different mutant cells occurred at much higher frequency than those of random controls (Supplemental Results; Figure S3B). These data suggest that the entire complex and its topoisomerase activity preferentially promote transcriptional repression of SRGs under starvation.

Third, the heatmaps made to compare the effects of the three mutant cells on SRGs (Figure 2D) displayed patterns very similar to their corresponding heatmaps for SAGs (Figure 1F). For example, all mutant lines showed more increased than decreased SRGs (5–18-fold) (Figure 2D, more red than blue colors). Moreover, the SRGs significantly increased in one mutant line had a strong preference to be increased in the other two lines (Figure 2D, see co-clustering of red color). In contrast, the SRGs decreased in one mutant line showed weaker tendency to be decreased in other two mutants (Figure 2D, see poor co-clustering of blue color). The data suggest that TOP3B, TDRD3 and the TOP3B topoisomerase activity have strong preference to coordinately repress transcription of SRGs.

Fourth, we performed calculations as described for SAGs in Figure 1G, and found that the SRGs that are significantly increased in one mutant cell line also preferentially exhibit the same direction of alteration (increase) in the two other mutant lines (Figure 2E). Specifically, for the 72 SRGs that show increased RNA-seq signals in *TOP3B-KO* cells, 46% and 39% of them exhibited the same direction of alteration in *TDRD3-KO* and *TOP3B-Y336F-KI* cells, respectively (Figure 2E); which are more than 10 folds higher than those showing the opposite direction of alteration (decrease) (4% and 1%, respectively) (Figure 2E). Similarly, for the 60 increased SRGs in *TDRD3-KO* cells, 55% of them exhibited the increase in *TOP3B-Y336F-KI* cells, whereas fewer than 1% showed decrease (Figure 2E, right). Moreover, the observed percentages of SRGs showing the same direction of alteration between each pair of mutant cell lines were 3–4-fold higher than those of random controls (Figure 2E, columns 1 versus 2). In contrast, the observed percentages of SRGs showing the opposite directions of alteration

were similar or lower than those of random controls (Figure 2E, columns 3–4). Together, these data suggest a strong preference for the TOP3B–TDRD3 complex and its topoisomerase activity to act coordinately—to promote not only transcriptional activation of SAGs, but also transcriptional repression of SRGs under starvation.

A Venn diagram made for the significantly increased SRGs (Figure 2F) resembles that for significantly decreases SAGs in the three mutant cells (Figure 1H), so that the conclusions drawn for SAGs can also be applied for SRGs. The number of SRGs increased in all three mutant cells ($n=24$) is similar to that of SAGs decreased in all mutant cells ($n=22$), suggesting that TOP3B–TDRD3 and its topoisomerase activity may use a mechanism that simultaneously enhance and repress transcription of similar numbers of genes. This suggestion is supported by findings that the percentages of SRGs that are significantly increased in each mutant cell line (12–14%) (Figure 2B) are similar to the percentages of SAGs that are decrease in the same mutant cell lines (10–15%) (Figure 1D).

TOP3B–TDRD3 regulates both basal and starvation-induced transcription

Analysis of several representative genes confirmed that starvation significantly increased RNA-seq signals of four SAGs (3–7 folds, $P < 0.05$) (*EGRI*, *FOS*, *JUN* and *AREG*) (Figure 3A, B, left), while decreased those of three SRGs (*KRT19*, *KCCN4* and *ADM*) (2–5-fold, $P < 0.05$) (Figure 3A, B, right). *GAPDH* gene was included as a control, whose RNA-seq level was not significantly altered (Figure 3A, right). Notably, the levels of 3 SAGs (*EGRI*, *FOS*, *JUN*, but not *AREG*) were significantly reduced ($P < 0.05$, 0.3–5-fold), whereas those of three SRGs were increased ($P < 0.05$, 0.3–2-fold) in starvation-treated *TOP3B-KO*, *TDRD3-KO* and *TOP3B-Y336F-KI* cells versus *WT-ST* cells (Figure 3A, B), consistent with the notion that TOP3B–TDRD3 and its topoisomerase activity can facilitate both transcriptional activation of the SAGs, and repression of the SRGs under starvation. For a subset of these genes (*EGRI* and *AREG* for SAGs; and *KRT19*, *KCCN4* for SRGs), their RNA levels were also significantly altered ($P < 0.05$, 0.3–5-fold) in nontreated *TOP3B-KO* cells in the same direction as those treated with starvation, suggesting that TOP3B also promotes basal transcription of these genes. The reduction of mRNA levels for the 4 representative SAG genes (*EGRI*, *FOS*, *AREG* and *DDIT4*) were subsequently confirmed by RT-qPCR (Figure 3C, D). As a control, the mRNA levels of the four SAGs were either unchanged or slightly increased in *FMRI* knockout cells, indicating that the effect of TOP3B–TDRD3 on SAGs is specific (Figure 3D).

To exclude the possibility that the findings from *TOP3B-KO* and *TDRD3-KO* (Figure 1–3) are due to off-target effects by CRISPR-Cas9 or clonal variation, we analyzed 3 representative SAGs in two new *KO* clones produced by different sgRNAs, *TOP3B-KO2* and *TDRD3-KO2*; and obtained largely consistent results (Supplemental Results; Figure S1A–C). Together, we observed a stimulatory effect of TOP3B–TDRD3 on starvation-activated transcription in two independent *TOP3B-KO*, 2 *TDRD3-KO*, and one *TOP3B-Y336F-KI*, but not in one *FMRI-KO* cell

lines. These data strongly suggest that the positive effect of TOP3B–TDRD3 on starvation-activated transcription is specific.

TOP3B can act in topoisomerase activity dependent and independent manners in transcription

Our heatmap and Venn diagram analysis revealed that a large fraction of SAGs or SRGs altered in *TOP3B-KO* cells do not show concomitant alteration in *TOP3B-Y336F* cells (~60%) (Figure 1H and Figure 2F), implying that TOP3B may regulate these genes in topoisomerase activity-independent manners. This notion is further supported by analyzing the total DEGs between the two cells (Supplemental Results and Figure S4). Examination of RNA-seq data revealed that 3 of the 4 representative SAGs that show reduced RNA levels in *TOP3B-KO* cells (*EGRI*, *FOS* and *DDIT4*) also exhibit reduction in *TOP3B-Y336F* cells, suggesting that these genes depend on its topoisomerase activity of TOP3B for transcription. One exception is *AREG* gene, whose RNA-seq levels were drastically reduced in *TOP3B-KO-ST* and *TDRD3-KO-ST* (by 80%), but only modestly reduced in *TOP3B-Y336F-ST* cells (by <20%) (Figure 3A, B). RT-qPCR (Figure 3D) showed that the reduction of *AREG* mRNA level is statistically significant in *TOP3B-KO*, *TDRD3-KO*, but not in *TOP3B-Y336F-KI* cells. The ChIP-seq data below show that TOP3B–TDRD3 can directly bind *AREG* gene, and TOP3B-inactivation reduces RNAPII-ser2p level in this gene (Figure 6A), indicating that *AREG* is directly bound and regulated by TOP3B–TDRD3 in a topoisomerase-independent manner. Together, these data suggest that TOP3B–TDRD3 depends on its topoisomerase activity to regulate some but not all its target genes.

To further study whether TOP3B depends on its topoisomerase activity to promote transcription, we ectopically-expressed TOP3B-WT or TOP3B-Y336F mutant in *TOP3B-KO* HCT116 cells (Figure 3E). We found that the mRNA levels of three representative SAGs (*EGRI*, *AREG* and *FOS*) are induced by starvation in both cells (Figure 3F), which mimics the findings in *WT* and *TOP3B-KO* cells (Figure 3C). Notably, the mRNA levels in *KO* cells ectopically expressing WT protein were significantly higher than those of cells expressing TOP3B-Y336F mutant or no TOP3B protein ($P < 0.05$; 2–3-fold) (Figure 3F), supporting the conclusion from *TOP3B-KO* and *Y336F-KI* cells that TOP3B depends on its topoisomerase activity to enhance transcription. One discrepancy was observed for *AREG*, which exhibited TOP3B topoisomerase activity-independence in *Y336F-KI* cells (Figure 3C, D), but dependence using the ectopic system (Figure 3F). Detailed explanation of these results and the discrepancy are in Supplemental Results.

TOP3B promotes starvation-induced redistribution of elongating RNAPII

To determine whether the observed mRNA level changes induced by either starvation or TOP3B inactivation occur at the transcription step, we performed ChIP-seq in *WT* and *TOP3B-KO* cells using one antibody against total RNAPII

(Supplemental Results and Figure S6), and another one against the elongating form of RNAPII, RNAPII-ser2p (Figure 4 and Supplementary Table S9). Our previous studies showed that *Top3b-KO* has stronger effects on RNAPII-ser2p than RNAPII-ser5p (the initiation form) (6), so that we will focus on the former below.

We found that RNAPII-ser2p signals were enriched with a large peak at the transcription end site (TES) and a small peak at transcription start site (TSS) (Figure 4A, B), which resemble with the published RNAPII-ser2p data (32), indicating validity of our assays. Heatmaps and metaplots showed that for the TOP3B-dependent SAGs, the overall levels of RNAPII-ser2p in *WT-ST* cells were higher than those of *WT-NT* cells (the largest peak was 100% higher) (Figure 4A, left; Figure 4B, top). In contrast, for the TOP3B-dependent SRGs, starvation reduced (more than 50%) the overall levels of RNAPII-ser2p (Figure 4A, right; Figure 4B, bottom). Notably, the level of RNAPII-ser2p for TOP3B-dependent SAGs in *TOP3B-KO-ST* cells was lower (about 50%) than those of *WT-ST* cells (Figure 4A, left; Figure 4B, top). In contrast, the levels of RNAPII-ser2p for TOP3B-dependent SRGs in *TOP3B-KO-ST* cells was higher (about 1.5-fold) (Figure 4A, right; Figure 4B, bottom). These data reveal a reciprocal pattern of RNAPII-ser2p alteration between SAGs and SRGs (Figure 4A, left versus right; Figure 4B, up vs. down): those of SAGs were increased in *WT-ST* but reduced in *TOP3B-KO-ST* cells; whereas those for SRGs were reduced in *WT-ST* but increased in *TOP3B-KO-ST* cell. This pattern is also confirmed by scatter plots containing data points from both SAGs and SRGs (Figure 4C, orange and blue, respectively), which clearly show patterns of reciprocal alterations in *WT-ST* vs. *WT-NT* cells, or in *TOP3B-KO-ST* versus *WT-ST* cells (data points of one color above whereas those of the other color below equal line). These data suggest that starvation and TOP3B may simultaneously enhance SAGs and suppress SRGs by facilitating redistribution of the elongating RNAPII—increasing it for SAGs and decreasing it for SRGs.

In support of this conclusion, the average RNAPII-ser2p signal changes at TES are statistically significant and exhibit the same reciprocal pattern of alteration for both SAGs and SRGs in *WT-ST* versus *WT-NT* cells, and in *TOP3B-KO-ST* versus *WT-ST* cells (Figure 4D). Together, our data suggest that the main effect of starvation and TOP3B–TDRD3 is on elongation of transcription.

TOP3B–TDRD3 preferentially binds TES regions of SAGs to enhance their transcription

To study whether TOP3B–TDRD3 directly acts on the SAGs or SRGs which they regulate, we performed ChIP-seq in *WT-NT* and *WT-ST* cells using antibodies against either TOP3B or TDRD3. Our attempt of using anti-TOP3B antibodies failed to produce any specific signals above those of a negative control—*TOP3B-KO* cells (data not shown). This result is consistent with our previous studies in mouse brains in which only anti-TDRD3 but not anti-TOP3B antibodies produced specific ChIP-signals (6). Because most if not all TOP3B and TDRD3 in cells are present in a stoichiometric complex (2), we used TDRD3 ChIP to identify

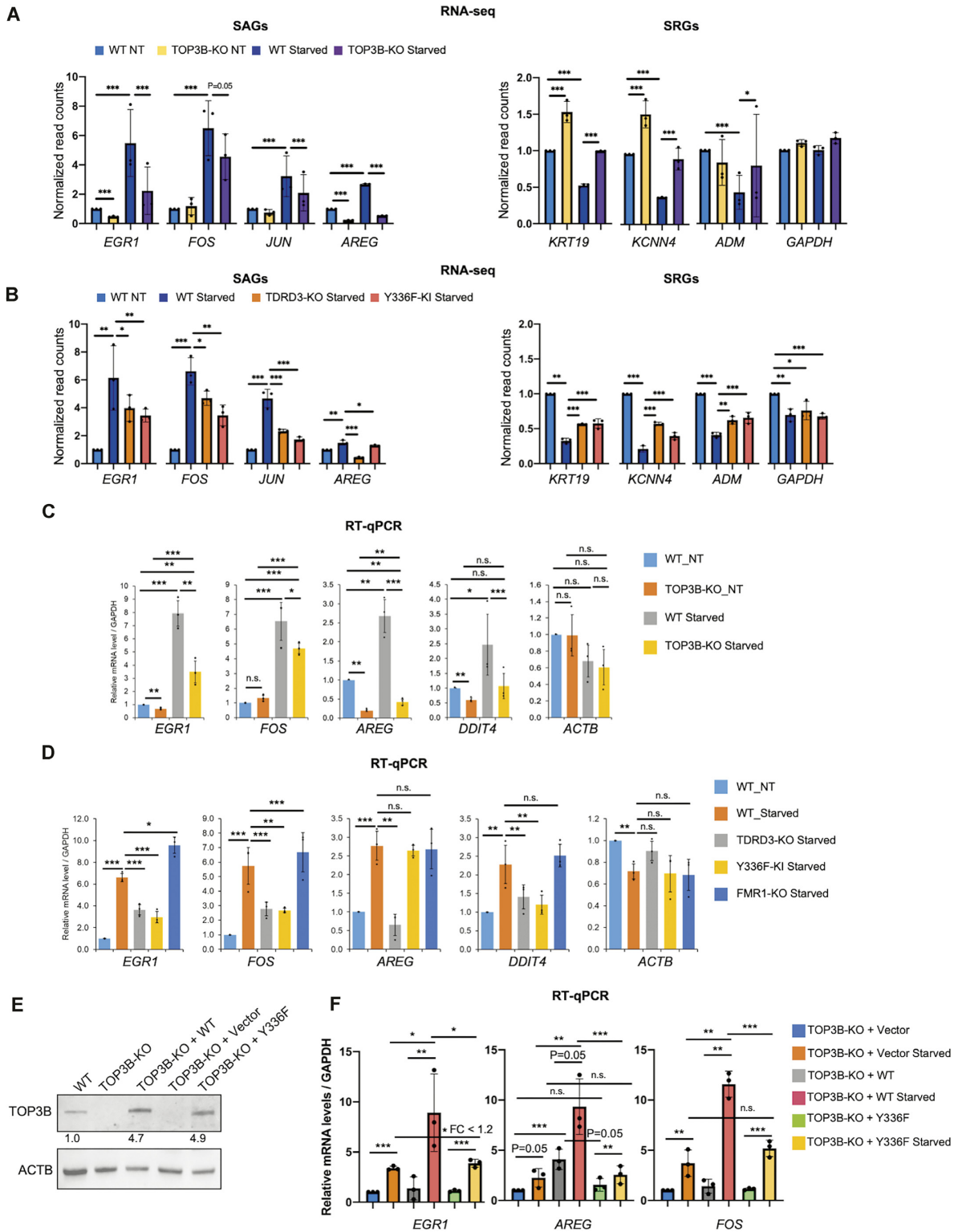


Figure 3. The representative SAGs and SRGs regulated by the TOP3B–TDRD3 complex. (A, B) The mRNA levels of four SAGs and three SRGs were detected by RNA-seq. *GAPDH* was a negative control here. The results were from three independent replicates. The p-values were calculated by DESeq2. (C, D) RT-qPCR verified the RNA levels of the representative SAGs and *ACTB* gene (a control). The data from *FMR1-KO* cells were shown here as negative controls. The starvation-induced transcription of these four genes was not dependent on FMRP. (E) Western blot detecting the protein levels of TOP3B and ACTB in different cell lines. TOP3B-KO + WT, TOP3B-KO + Vector, TOP3B-KO + Y336F were three cell lines generated with a retrovirus vector system based on *TOP3B-KO* HCT116 cells. WT, ectopically-expressed wild type TOP3B; Vector, pBAGE-puro vector only without transgene; Y336F, ectopically-expressed TOP3B-Y336F. The numbers in the middle are the relative protein levels measured by ImageJ. (F) RT-qPCR measuring the mRNA levels of three representative genes in the cell lines (E) with or without starvation. ****P* < 0.001; ***P* < 0.01; **P* < 0.05; n.s., not significant (*n* = 3, two-tailed Student's *t*-test). Graphs generated using *P*-values by ANOVA test are shown in Supplementary Figure S8.

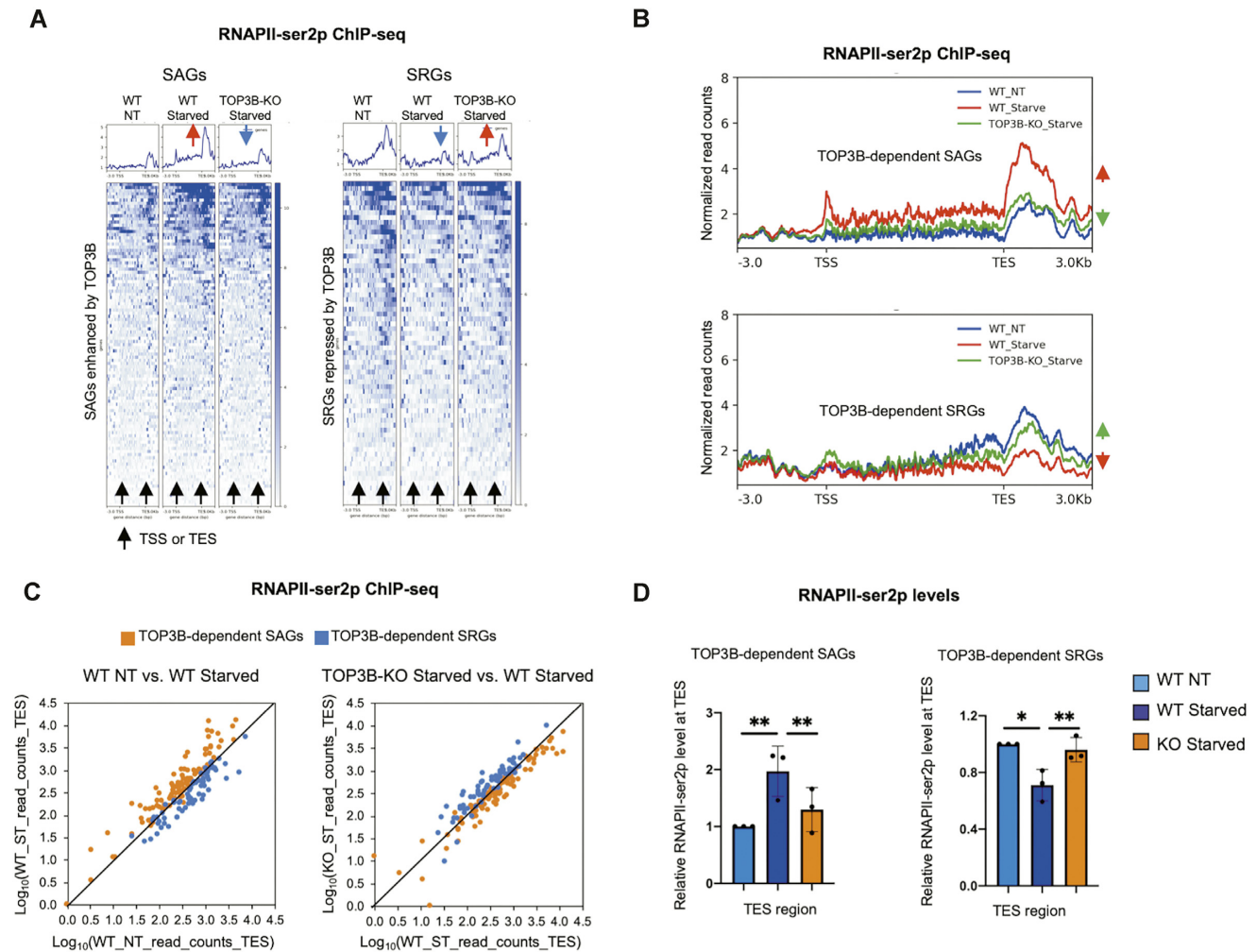


Figure 4. TOP3B promotes starvation-induced redistribution of elongating RNAPII. (A) Average ChIP-seq signal profiles (top) and heatmaps (bottom) depicting the RNAPII-ser2p ChIP-seq signals on TOP3B-dependent SAGs (left) and SRGs (right). Blue arrows represent reduced, whereas red arrows represent increased RNAPII-ser2p signals. (B) Average ChIP-seq signal profiles depicting the RNAPII-ser2p levels on TOP3B-dependent SAGs (up) and SRGs (down). The up and down arrows on the right represent upregulated and downregulated RNAPII-ser2p levels separately. (C) Scatter plots showing the comparisons of the RNAPII-ser2p levels of TOP3B-dependent SAGs (orange) and SRGs (blue) in *WT* or *TOP3B-KO* cells. (D) The averages of the RNAPII-ser2p ChIP-seq normalized read counts at TES regions of TOP3B-dependent SAGs or SRGs from three independent experiments were used to calculate. *** $P < 0.001$; ** $P < 0.01$; * $P < 0.05$; n.s., not significant ($n = 3$, two-tailed Student's t -test). Graphs generated using p-values by ANOVA test are shown in Figure S8.

the targets of the TOP3B–TDRD3 complex. We included a critical negative control: mock ChIP-seq from *TDRD3-KO* cells under the same conditions, to exclude non-specific signals due to antibody cross-reactivity. Heatmaps and metaplots revealed a sharp peak of TDRD3 signals at TSS of all genes in *WT-NT* and the negative control cells (Figure 5A left), suggesting that this peak should be largely non-specific due to the artifactual ‘hotspots’ (33). In *WT-ST* cells, the largest TDRD3 peak was present in the TSS, whereas a smaller peak at a region immediately downstream of the TES (Figure 5A, right). Because both peaks are higher than those in the negative controls (about 2 folds), they should contain signals derived from TOP3B–TDRD3. We selected TDRD3 peaks in *WT* cells that are 1.5-fold higher than those of negative controls in two independent experiments as potential TOP3B–TDRD3-binding sites, and identified about 70 TDRD3 peaks in *WT-NT* cells, and about 10-fold

more (700) peaks in *WT-ST* cells (Figure 5B and Supplementary Table S7). These peaks are localized at TSS (50%) and TES (6%) (Figure 5B). The findings that there are 10-fold more TDRD3 peaks in *ST* than *NT* cells suggest that TOP3B–TDRD3 regulates more genes in activated than basal transcription, consistent with our early finding (6).

Based on earlier data that TOP3B–TDRD3 exhibits increased binding to their target genes in response to neuronal activity (6), we hypothesize that the complex that regulates starvation-induced transcription may also show starvation-enhanced binding to its targets. We therefore selected TDRD3 peaks that show increased levels in *WT-ST* versus *WT-NT* cells (>1.5-fold), and identified about 111 TDRD3 peaks localized in 67 protein-coding genes (Figure 5C and Supplementary Table S7), at TSS, TES and other regions. Metaplots revealed that the TDRD3 peaks at TSS and TES of these genes have higher signal-to-background

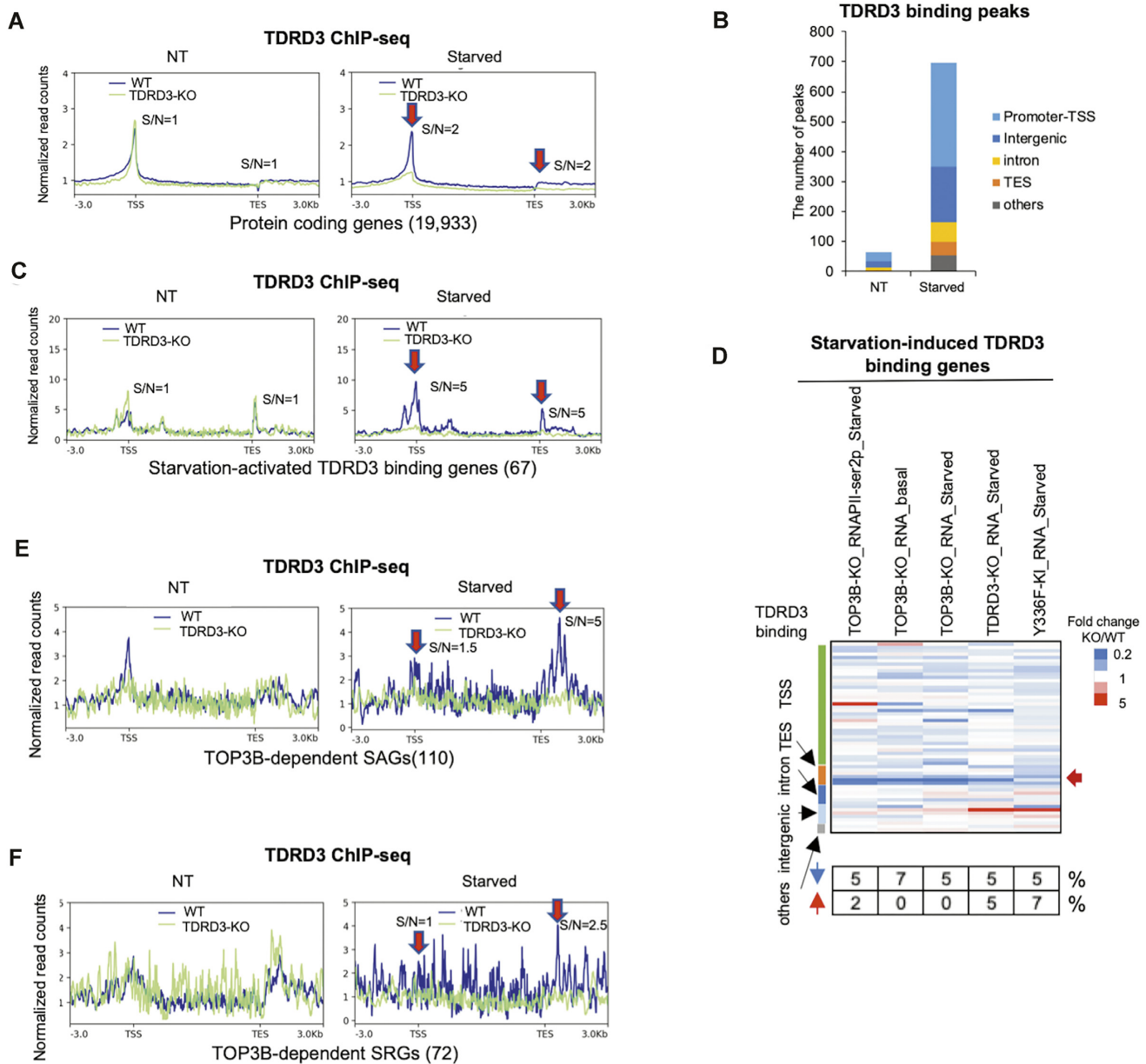


Figure 5. Cell starvation increases TDRD3 binding mainly to TES regions of the TOP3B-dependent SAGs. (A) Average of TDRD3 occupancy on protein coding genes (19 933) in *WT* and *TDRD3-KO* cells under no treatment (NT) or starvation (Starved) condition. S/N, TDRD3 ChIP Signals / Noise ratio. The red arrows marked TDRD3 peaks. (B) The annotation of TDRD3 binding peaks under no treatment or starvation condition by MACS2 and HOMER. (C) Average of TDRD3 occupancy on the starvation-induced TDRD3 binding genes (67) (normalized by RPKM). Two major peaks were identified (one was at TSS, the other was at TES). (D) The fold changes of mRNA and RNAPII-ser2p levels on the starvation-induced TDRD3 binding genes between *WT* and different mutant cells. The reduced genes were in blue color and the increased gene in red color. The percentages of the DEGs (fold change > 1.5) were marked below. The blue arrow represents reduction. The red arrow (left) represents increase. The red arrow on the right marks the genes bound by TDRD3 at TES region. (E, F) Average of TDRD3 occupancy on TOP3B-dependent SAGs (E) or SRGs (F) in *WT* and *TDRD3-KO* cells under no treatment (NT) or starvation (Starved) condition. The peak of TOP3B-dependent SAGs at TES was induced by starvation and was higher in *WT* than that in *TDRD3-KO* cells. The peak at TSS was not induced by starvation and the height was comparable between *WT* and *TDRD3-KO* cells. The TDRD3 binding signals of TOP3B-dependent SRGs were higher in *WT* cells than *TDRD3-KO* cells under starvation. However, there was no obvious peaks found for SRGs. These results can be observed in two different biological replicates.

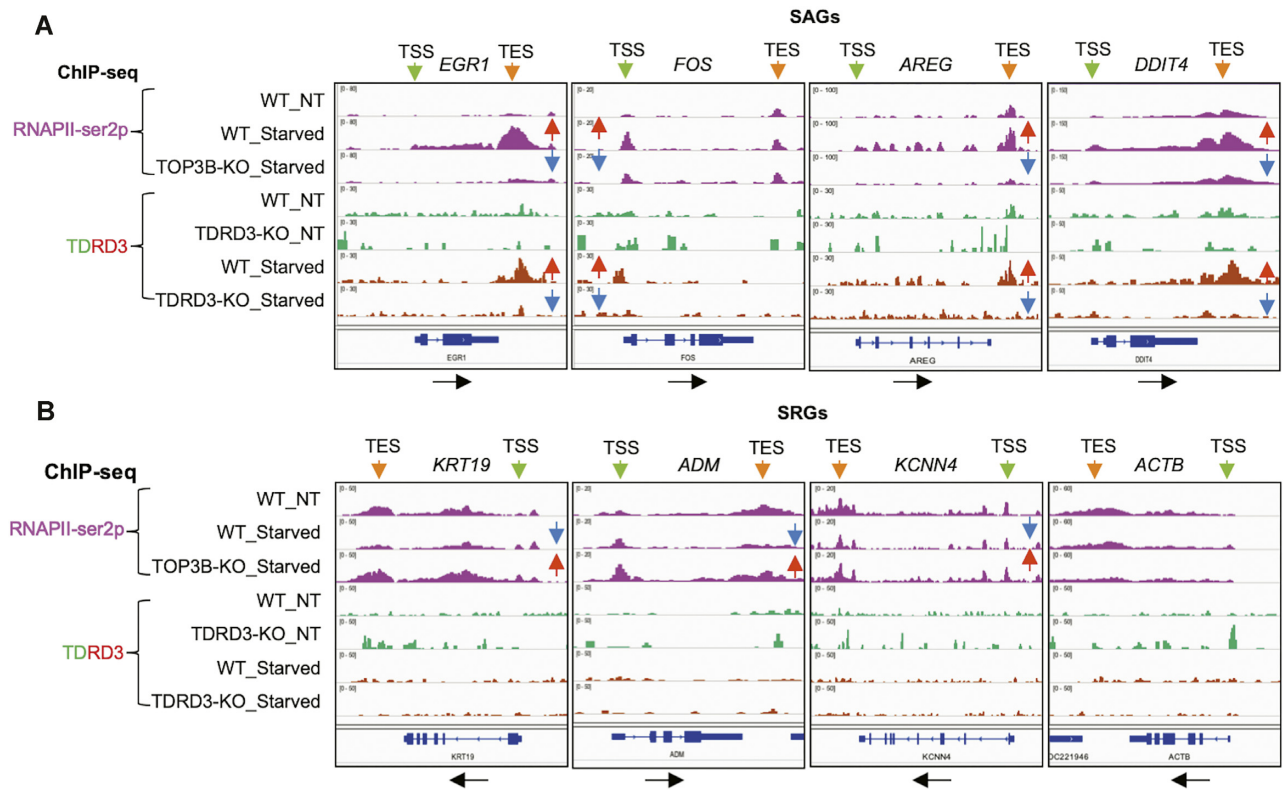


Figure 6. The TOP3B–TDRD3 complex co-localizes with elongating RNAPII and promotes starvation-induced RNAPII redistribution. (A) Genome browser representations of ChIP-seq normalized reads for RNAPII-ser2p and TDRD3 at the *EGR1*, *FOS*, *AREG* and *DDIT4* gene loci in *WT* and *TOP3B-KO* cells nontreated (NT) or treated with starvation (Starved). The black arrows below marked transcriptional direction. The green and orange arrows above marked TSS and TES regions separately. The red and blue arrows in the middle marked the increased and decreased ChIP-seq signals separately. (B) Genome browser representations of ChIP-seq normalized reads for RNAPII, RNAPII-ser2p and TDRD3 at the *KRT19*, *ADM*, *KCNN4* and *ACTB* gene loci in *WT* and *TOP3B-KO* cells. These data can be observed at least in two replicates. One of the representative results were shown here. For individual gene and one type of ChIP-seq data, the min and max values of Y-axis are the same.

difference in *WT-ST* than *WT-NT* cells (Figure 5C, compare two plots), confirming that TDRD3 binding is enhanced by starvation. Comparing to the transcriptional data derived from RNAPII ChIP-seq and RNA-seq showed that among these 67 genes, those with TDRD3 binding at TSS or TES (but not introns or intergenic regions) display an overall reduced transcription by RNA-seq and RNAPII-ser2p ChIP-seq assays of *TOP3B-KO*, *TDRD3-KO* and *Y336F-KI* cells (Figure 5D, heatmap, more blue color than red). In addition, they contained more significantly decreased (5–7%) than increased DEGs (0–2%) from *TOP3B-KO* cells. In particular, the genes with TDRD3 binding at the TES region showed consistently reduced transcription signals in all three mutant cells (Figure 5D marked by red arrow), suggesting that TOP3B–TDRD3 can bind TES of these genes and promote their transcription in topoisomerase activity-dependent manner.

We then investigated whether TOP3B-dependent SAGs and SRGs are enriched with TDRD3-binding genes. Metaplots failed to detect TDRD3 peaks that are significantly higher than the negative control (>1.5-fold) for TOP3B-dependent SAGs or SRGs under basal conditions (Figure 5E, F, left). Notably, under starvation, metaplots detected a sharp TDRD3 peak at TES and a small peak at TSS region of TOP3B-dependent SAGs (Figure 5E right). And both peaks are higher than those signals from nega-

tive control group (5-fold) (Figure 5E right), which mimics the findings from analysis of starvation-induced TDRD3 binding genes (Figure 5C, right), suggesting that starvation-induced TOP3B–TDRD3 binding at TES regions can preferentially enhance transcriptional activation of TOP3B-dependent SAGs, and this effect is likely direct. Conversely, for TOP3B-dependent SRGs, the TDRD3 were randomly distributed from –3 kb upstream of TSS to 3kb downstream of TES; and not enriched at TSS or TES (Figure 5F). These data imply that TOP3B–TDRD3 may indirectly affect transcription of TOP3B-dependent SRGs.

TOP3B–TDRD3 co-localizes with and regulates redistribution of elongating RNAPII

We examined several representative SAGs (Figure 3A) to determine whether TOP3B–TDRD3 displays starvation-induced binding, and whether its binding sites colocalize with those of RNAPII-ser2p, as predicted by the Metaplot (Figure 5E). For three of the four TOP3B-dependent SAGs (*EGR1*, *AREG* and *DDIT4*), we observed starvation-induced TDRD3 binding peaks near TES regions; and these peaks co-localized with those of RNAPII-ser2p (Figure 6A, *WT-ST* versus *WT-NT* cells). For *FOS* gene, the TDRD3 was detected at TSS, which also overlaps with RNAPII-ser2p (Figure 6A). For the 3 TOP3B-dependent

SRGs, we did not detect specific TDRD3 binding peaks (Figure 6B), which is consistent with the metaplot above (Figure 5F).

UCSC browser plots of the four representative TOP3B-dependent SAGs and three SRGs also confirmed the effect of TOP3B inactivation on distribution of RNAPII-ser2p (Figure 6A, B). For three of the four SAGs (*EGR1*, *AREG* and *DDIT4*), the RNAPII-ser2p peaks at the TSS region, gene bodies, and/or TES, were all enhanced by starvation, and suppressed in *TOP3B-KO* cells. The single exception is *FOS* gene, whose RNAPII-ser2p level was only increased by starvation and reduced by *TOP3B-KO* at TSS but not TES, suggesting that this gene could be regulated by a different mechanism, possibly at the initiation step. For the 3 SRGs (*KRT19*, *KCNN4* and *ADM*), their RNAPII-ser2p signals were consistently reduced by starvation and increased by *TOP3B-KO* cells. The RNAPII-ser2p level changes regulated by TOP3B could be observed in three replicates (Supplementary Figure S2E, F). We also analyzed RNAPII ChIP-seq data for the same representative SAGs and SRGs, and the results (Supplemental Results; Figure S6A, B) are largely consistent with those of RNAPII-ser2p (Figure 6A, B), thus supporting our model. Together, these data support a model that TOP3B-TDRD3 may interact with and regulates distribution of elongating RNAPII in starvation-induced transcription (see Discussion below).

TOP3B knockout alters transcription of autophagy-associated genes and reduces autophagy

Our data above demonstrated that two transcriptional regulators of autophagy genes, *EGR1* (20) and *FOS* (34), exhibit reduced transcription in *TOP3B-KO-ST* cells (Figures 3A, C and 6A). This led us to determine whether any autophagy genes are also regulated by TOP3B (20). We found that 10 and 5 autophagy genes were significantly decreased and increased, respectively, in *TOP3B-KO-ST* cells (vs. *WT-ST* cells) (Supplementary Table S8). Analysis of three representative autophagy-associated genes (*MAP1LC3B*, *DDIT3* and *PPP1R15A*) showed that their RNA-seq levels were increased in *WT-ST* versus *WT-NT* cells, and reduced in *TOP3B-KO-ST* versus *WT-ST* cells (Figure 7A, B). Moreover, their RNAPII-ser2p levels were also increased *WT-ST* versus *WT-NT* cells, and the decreased in *TOP3B-KO-ST* versus *WT-ST* cells (Figure 7C, D). TDRD3 ChIP-seq detected a peak at TSS of *MAP1LC3B* gene in one replicate (Figure 7C), but failed to detect any peaks above background in the other two genes, indicating that TOP3B may regulate these autophagy-associated genes indirectly.

We performed immunoblotting of MAP1LC3B, and observed that one of its two isoforms (LC3B-I) exhibited significantly reduced levels in *TOP3B-KO-ST* cells at 4 and 6 h post-starvation (Figure 7E; Figure 7F, left). The other isoform (LC3B-II) exhibited a strong trend of reduction ($P = 0.08$) at 6 h post starvation, although the difference does not reach statistical significance (Figure 7E; Figure 7F, right). Together, these data support that notion that TOP3B is required for normal transcription of a fraction of autophagy genes.

We studied whether *TOP3B-KO* cells have reduced autophagy by LysoTracker staining, a common method for

autophagy detection (35). LysoTracker signals in *WT-ST* and *TOP3B-KO-ST* HCT116 cells were significantly higher at 3 and 6 h post-starvation than those in their corresponding non-treated cells (Figure 8A, B), consistent with the previous reports that starvation can induce autophagy (20,36). Interestingly, the LysoTracker signals in *TOP3B-KO-ST* cells were significantly lower than those of *WT-ST* cells at 6 h post-starvation, suggesting that *TOP3B* inactivation reduces starvation-induced autophagy (Figure 8A, B).

We also performed LysoTracker staining in the fat body of *Top3b* mutant *Drosophila*, which has been previously used to dissect the autophagy pathways (35). Consistent with earlier reports, the LysoTracker signals were significantly higher in *WT Drosophila* fat body treated with starvation than those without the treatment, indicating normal activation of autophagy by starvation (Figure 8C, D). Importantly, the LysoTracker signals in fat body of *Top3b* knockout (*Top3b^{-/-}*) flies were significantly lower than those of *WT* flies under starvation; and were indistinguishable to those of non-starved flies (Figure 8C, D), indicating reduced autophagy induction in *Top3b* mutant cells.

DISCUSSION

TOP3B-TDRD3 and its topoisomerase activity act coordinately in transcription

We have recently shown that TOP3B and TDRD3 work coordinately to regulate translation and turnover for specific mRNAs in HCT116 cells (9). Here, we demonstrate that they also coordinately regulate starvation-induced transcription. The data thus imply that the entire TOP3B-TDRD3 complex facilitates a wide range of cellular process on both DNA and mRNAs in cells.

We have previously found that TOP3B-TDRD3 can act in either topoisomerase-activity dependent or independent manners when regulating mRNA translation and turnover (9). Here we report evidence that the complex can function in both manners when regulating transcription (see representative genes in Figure 3C, D and Figure 6A). Action in a topoisomerase-activity independent manner was not totally unexpected, because TOP1 has been reported to regulate transcription in topoisomerase activity-independent pathways (37,38). TOP3B not only possesses topoisomerase activity, but also a binding activity to ssRNA and ssDNA through its RGG-domain and Zn-finger domain (2,13,39). In addition, TDRD3 has been reported to interact with RNAPII and its mediator complex (15,40). It is therefore possible that TOP3B-TDRD3 can regulate transcription through these other interactions.

Our analysis of total DEGs in *TOP3B-KO*, *TDRD3-KO* and *TOP3B-Y336F-KI* cells (Supplemental Results and Figure S4) showed that TOP3B-TDRD3 and its catalytic activity preferentially enhance highly expressed genes, which are consistent with previous findings in mouse brains (6). This feature is shared by TOP1 and TOP2 (1,41). Moreover, TOP3B preferentially enhances transcription of long genes (Supplemental Results and Figure S4). This feature also resembles those of TOP1 and TOP2 (42). The data imply that long and highly expressed genes tend to have complex topological problems whose resolution may require combined actions by all three families of topoisomerases.

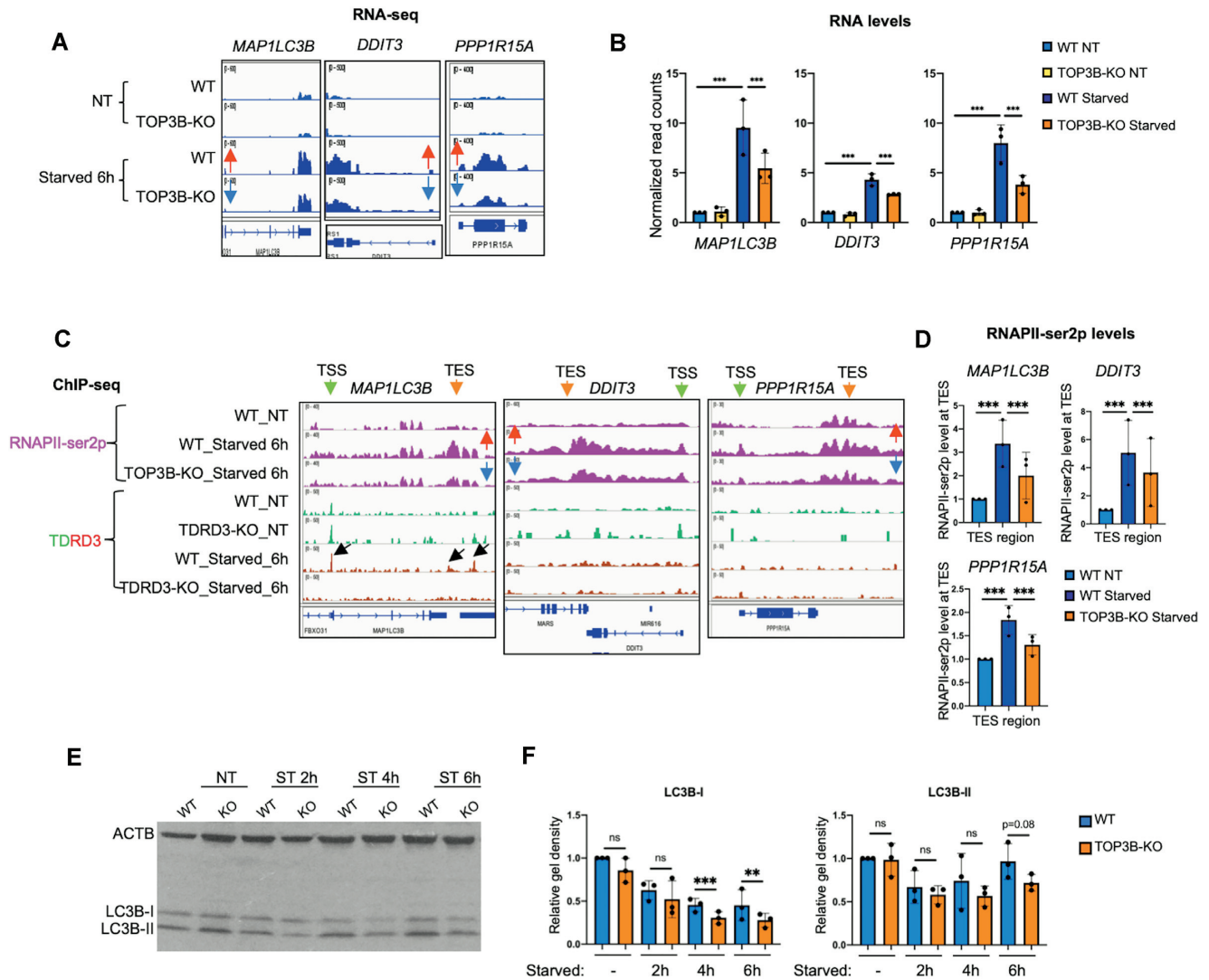


Figure 7. TOP3B knockout alters the transcription of autophagy-associated genes. (A) Genome browser representations of RNA-seq normalized reads at the three gene loci (*MAP1LC3B*, *DDIT3* and *PPP1R15A*). The induction of these three autophagy-associated genes were dependent on TOP3B. Red and blue arrows in the middle represent increased and decreased mRNA levels separately. (B) Bar graphs generated using normalized read counts of RNA-seq (three independent replicates) show the RNA levels of the representative genes. $***P < 0.001$. The *P*-values were calculated by DESeq2. (C) Genome browser representations of ChIP-seq (RNAPII-ser2p and TDRD3) normalized reads at the three gene loci (*MAP1LC3B*, *DDIT3* and *PPP1R15A*). Starvation increased and *TOP3B-KO* reduced the binding of RNAPII-ser2p on these three gene loci, suggesting that the transcription of these three genes was promoted by TOP3B. TDRD3 binding peaks were observed at TSS and TES regions of *MAP1LC3B* gene in one replicate. No TDRD3 binding peak was found at *DDIT3* and *PPP1R15A* gene loci. (D) Bar graphs generated using normalized read counts of RNAPII-ser2p ChIP-seq (three independent replicates) show the RNAPII-ser2p levels of the representative genes at TES regions. $***P < 0.001$. The *p*-values were calculated by DESeq2. (E) Western blotting shows the protein levels of LC3B-I/II and ACTB in *WT* and *TOP3B-KO* cells under no treatment (NT) and starved for 2, 4, 6 h conditions. (F) Western blotting band densities of three independent experiments were measured by ImageJ. $***P < 0.001$; $**P < 0.01$; $*P < 0.05$; n.s., not significant ($n = 3$, two-tailed Student's *t*-test). Graphs generated using *P*-values by ANOVA test are shown in Supplementary Figure S8.

TOP3B–TDRD3 promotes transcription induced by environmental stimuli

While we have previously shown that TOP3B–TDRD3 can promote neuronal activity-activated transcription in mouse brains (6), its roles in transcription within non-neuronal cells had remained unestablished. Here we demonstrate that TOP3B–TDRD3 can directly bind a fraction of SAGs and enhance their transcription in a non-neuronal cell line, HCT116, suggesting that this topoisomerase may promote transcription in a broad range of cells and tissues as do other topoisomerases (1,43). This is consistent with studies

of *Top3b-KO* mice that show several phenotypes unrelated to neurons, including autoimmunity and shortened lifespan (21,44).

Similar to our previous findings in mouse brains, we found that in HCT116 cells, TOP3B–TDRD3 regulates fewer genes in basal compared to stimulated conditions, suggesting that TOP3B–TDRD3 mainly promotes transcriptional activation induced by environmental stimuli. This ability resembles that of TOP1 and TOP2(A or B) (45–49). It seems likely that stimuli-induced transcription may cause a rapid rise of different types of

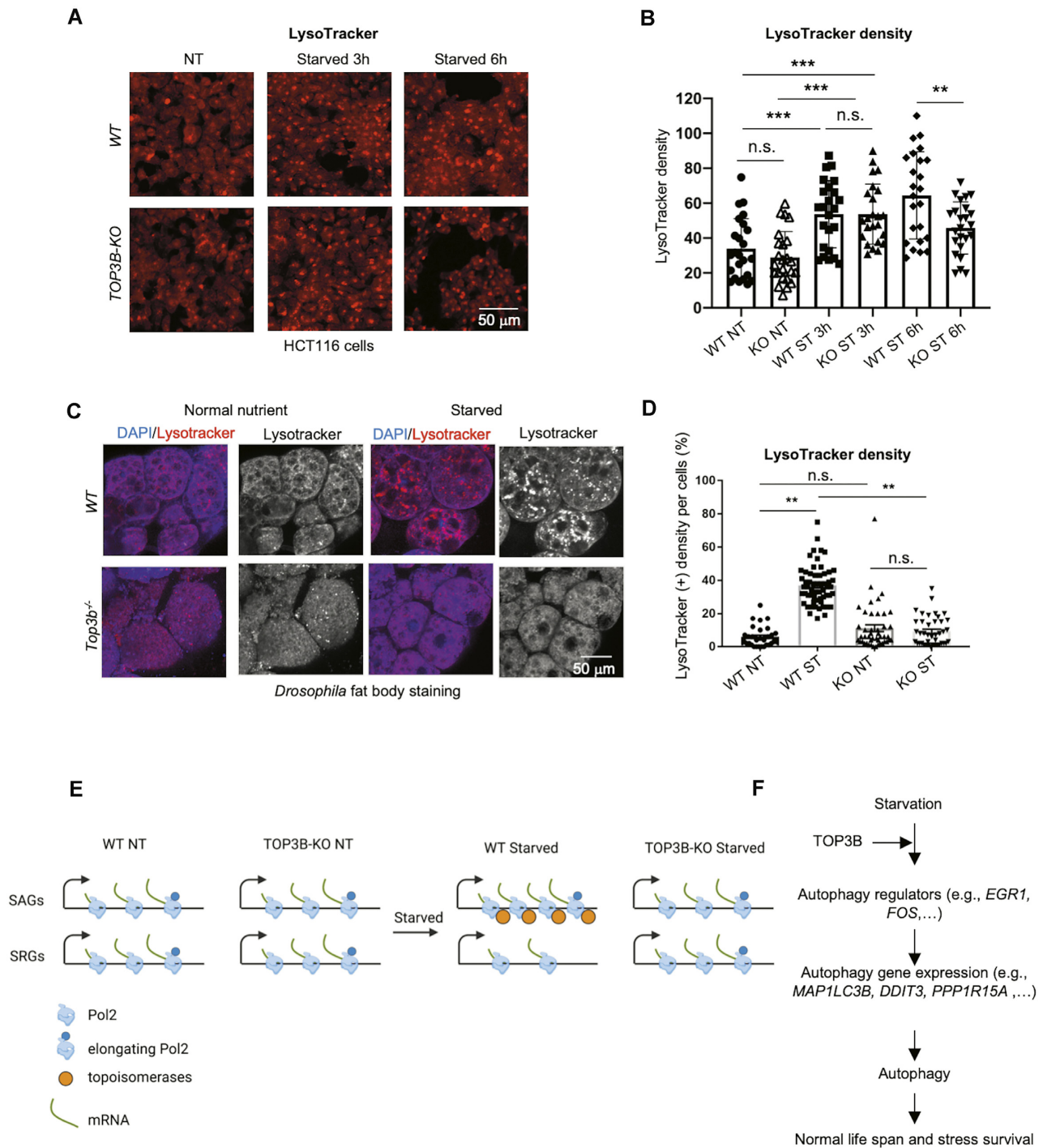


Figure 8. TOP3B knockout reduces starvation-induced autophagy. (A, B) *WT* and *TOP3B-KO* HCT116 cells without treatment (NT) or treated with EBSS for 3 or 6 h were incubated with 1 μ M LysoTracker for 20 min, followed by fixation. The images were captured using confocal microscope (A). The density of LysoTracker was measured by ImageJ (B). (C, D) *WT* and *Top3b^{-/-}* flies were fed with normal nutrient or starved for 6 h. The fat bodies were stained with LysoTracker or DAPI followed by fixation. The images were captured using confocal microscope (C). The density of LysoTracker was measured by ImageJ (D). *** $P < 0.001$; ** $P < 0.01$; * $P < 0.05$; n.s., not significant ($n = 3$, two-tailed Student's *t*-test). Graphs generated using *P*-values by ANOVA test are shown in Supplementary Figure S8. (E) A cartoon showing that TOP3B–TDRD3 was recruited to SAGs under starvation to enhance their transcription and RNAPII levels. TOP3B-KO reduced RNAPII level on SAGs but passively increased RNAPII level on SRGs. (F) A model shows the function of TOP3B in starvation-induced autophagy. Under starvation, TOP3B–TDRD3 is recruited to autophagy regulators (such as *EGR1* and *FOS*) gene loci to enhance their transcription. These autophagy regulators further activate expression of autophagy-associated genes (such as, *MAP1LC3B*, *DDIT3*). The activation of the autophagy-associated genes further facilitates autophagy process. TOP3B may facilitate normal life span and stress survival of animals by enhancing autophagy.

topological stress that may be resolved by different topoisomerases.

TOP3B–TDRD3 can enhance or suppress transcription by regulating elongating RNAPII distribution

We discovered that the effect of TOP3B–TDRD3 on transcription can be either positive or negative—it can enhance transcription of SAGs while suppressing transcription of SRGs. The findings that TOP3B can enhance starvation-activated transcription mimics our earlier results that TOP3B can stimulate neuronal activity-activated transcription (6); and are also in accord with the prevailing idea that topoisomerases typically enhance transcription by relaxing supercoils produced by RNA polymerases (1). However, suppression of transcription at some sites by TOP3B has not been observed before. Our findings that TOP3B can repress transcription resemble several previous studies for TOP1 and TOP2, which revealed similar suppressive effects on transcription (37,50–52). The data thus suggest that all three family of topoisomerases can regulate transcription in both positive and negative manners.

Mechanistic studies revealed a striking similarity between TOP3B–TDRD3 and elongating RNAPII in their binding to SAGs. Both of them display strongly increased binding in response to starvation (Figures 4A, B, 5C, 6A), and their binding sites overlap at the TES regions of SAGs. To our knowledge, this is the first report of a topoisomerase that binds TES sequences. In support of this inference, we reanalyzed our data from mouse brains (6) and detected TOP3B–TDRD3 binding at TES as well (in addition to TSS) (Supplementary Figure S7). Thus, TOP3B–TDRD3 may directly interact with elongation RNAPII to increase its levels at SAGs, which is in agreement with the reports that TDRD3 can directly interact with RNAPII (15,40). In addition, our preliminary data suggest that TOP1 can also bind TES regions under starvation (Su et al., manuscript in preparation). Since both TOP3B and TOP1 have been reported to interact with RNAPII (15,43), and elongating RNAPII (RNAPII-ser2p) is enriched at TES regions, our data suggest that TOP3B and TOP1 can associate with elongating RNAPII to promote transcriptional elongation under starvation.

As for TOP3B-dependent SRGs, we did not observe specific peaks of TOP3B–TDRD3 at either TSS or TES (Figure 5F and Figure 6B), suggesting that TOP3B–TDRD3 may indirectly regulate their RNAPII-ser2p levels (Figure 8E). We propose a model that TOP3B–TDRD3 may simultaneously enhance and suppress starvation-induced transcription for SAGs and SRGs, respectively, by altering the distribution of elongating RNAPII (Figure 8E). In response to starvation, RNAPII-ser2p or other transcription factors may become redistributed—removed from SRGs and associated with SAGs, leading to simultaneous repression of the former and activation of the latter genes. TOP3B–TDRD3 may facilitate this process by direct binding and traveling with elongation RNAPII in SAGs to relax supercoils generated in transcriptional elongation. The relaxing of supercoils may then stabilize the association between RNAPII and templates, so that the levels of RNAPII-ser2p are increased at SAGs. When TOP3B–TDRD3 topoisomerase

activity is inactivated, the accumulation of supercoils in SAGs may lead to RNAPII dissociation from SAGs, which may become associated with SRGs, leading to reduced transcription for the former and increased transcription for the latter.

TOP3B–TDRD3 promotes transcription of IEGs and autophagy

We found that the SAGs dependent on TOP3B–TDRD3 action include several critical IEGs (immediate early genes, *EGR1*, *FOS* and *JUN*), and stress response genes (*AREG* and *DDIT4*). These IEGs have also been shown to depend on TOP3B and TOP2B for neuronal activity-activated transcription in mouse brain (6,53). The reduced transcription of IEGs and stress response genes in TOP3B–TDRD3 mutant cells and mice suggest that TOP3B–TDRD3 could be important for organisms to adapt to different environmental cues and to stress. Consistent with this notion, we found that starvation-retreated *TOP3B-KO* HCT116 cells exhibit decreased transcription of several autophagy genes (Figure 7A–F). Moreover, both *TOP3B-KO* HCT116 cells and *Drosophila* fat body show reduced autophagy (Figure 8A–D). Our ChIP-seq data (Figure 7C) revealed that TOP3B–TDRD3 shows no reproducible binding to the autophagy genes that it regulates, suggesting that its stimulation of transcription of autophagy genes is likely indirect. In this regard, we noted that the two IEGs directly bound and regulated by TOP3B–TDRD3, *EGR1* and *FOS*, encode transcription factors that can enhance expression of autophagy genes (20,34). We therefore propose that TOP3B–TDRD3 may facilitate autophagy through a signaling cascade (Figure 8F): in response to starvation, TOP3B–TDRD3 may directly enhance transcription of *EGR1* and *FOS* genes whose gene products subsequently promote transcription of downstream autophagy genes, leading to increased autophagy. Because autophagy is required for normal life span and stress survival (18,22,54), its reduction may contribute to the shortened lifespan of *Top3b-KO* mice (21).

DATA AVAILABILITY

All next-generation sequencing data were deposited at GEO, and the accession number is GSE214322.

SUPPLEMENTARY DATA

Supplementary Data are available at NAR Online.

ACKNOWLEDGEMENTS

We thank Dr David Schlessinger, Tianyi Zhang and Xingliang Zhu for critical reading of the manuscript. This work utilized the computational resources of the NIH HPC Biowulf Cluster and NIA computer servers.

Author contributions: S.S., Y.X. and S.K.L. performed most of the experiments with assistance from Y.Z., A.S., J.F., S.D. and W.W. S.S. and W.W. designed the experiments. S.S. and W.W. wrote the manuscript. All authors commented on the manuscript.

FUNDING

Intramural Research Program of the National Institute on Aging, National Institutes of Health [Z01 AG000657-08]. Funding for open access charge: National Institute on Aging [Z01 AG000657-08].

Conflict of interest statement. None declared.

REFERENCES

- Pommier, Y., Sun, Y., Huang, S.N. and Nitiss, J.L. (2016) Roles of eukaryotic topoisomerases in transcription, replication and genomic stability. *Nat. Rev. Mol. Cell Biol.*, **17**, 703–721.
- Xu, D., Shen, W., Guo, R., Xue, Y., Peng, W., Sima, J., Yang, J., Sharov, A., Srikantan, S., Yang, J. *et al.* (2013) Top3beta is an RNA topoisomerase that works with fragile X syndrome protein to promote synapse formation. *Nat. Neurosci.*, **16**, 1238–1247.
- Ahmad, M., Xue, Y., Lee, S.K., Martindale, J.L., Shen, W., Li, W., Zou, S., Ciaramella, M., Debat, H., Nadal, M. *et al.* (2016) RNA topoisomerase is prevalent in all domains of life and associates with polyribosomes in animals. *Nucleic Acids Res.*, **44**, 6335–6349.
- Siaw, G.E., Liu, I.F., Lin, P.Y., Been, M.D. and Hsieh, T.S. (2016) DNA and RNA topoisomerase activities of Top3beta are promoted by mediator protein Tudor domain-containing protein 3. *Proc. Natl. Acad. Sci. U.S.A.*, **113**, E5544–E5551.
- Ahmad, M., Xu, D. and Wang, W. (2017) Type IA topoisomerases can be “magicians” for both DNA and RNA in all domains of life. *RNA Biol.*, **14**, 854–864.
- Joo, Y., Xue, Y., Wang, Y., McDevitt, R.A., Sah, N., Bossi, S., Su, S., Lee, S.K., Peng, W., Xie, A. *et al.* (2020) Topoisomerase 3beta knockout mice show transcriptional and behavioural impairments associated with neurogenesis and synaptic plasticity. *Nat. Commun.*, **11**, 3143.
- Saha, S., Yang, X., Huang, S.N., Agama, K., Baechler, S.A., Sun, Y., Zhang, H., Saha, L.K., Su, S., Jenkins, L.M. *et al.* (2022) Resolution of R-loops by topoisomerase III-beta (TOP3B) in coordination with the DEAD-box helicase DDX5. *Cell Rep.*, **40**, 111067.
- Yang, Y., McBride, K.M., Hensley, S., Lu, Y., Chedin, F. and Bedford, M.T. (2014) Arginine methylation facilitates the recruitment of TOP3B to chromatin to prevent R loop accumulation. *Mol. Cell*, **53**, 484–497.
- Su, S., Xue, Y., Sharov, A., Zhang, Y., Lee, S.K., Martindale, J.L., Li, W., Ku, W.L., Zhao, K., De, S. *et al.* (2022) A dual-activity topoisomerase complex regulates mRNA translation and turnover. *Nucleic Acids Res.*, **50**, 7013–7033.
- Prasanth, K.R., Hirano, M., Fagg, W.S., McAnarney, E.T., Shan, C., Xie, X., Hage, A., Pietzsch, C.A., Bukreyev, A., Rajsbaum, R. *et al.* (2020) Topoisomerase III-beta is required for efficient replication of positive-sense RNA viruses. *Antiviral Res.*, **182**, 104874.
- Saha, S., Sun, Y., Huang, S.N., Baechler, S.A., Pongor, L.S., Agama, K., Jo, U., Zhang, H., Tse-Dinh, Y.C. and Pommier, Y. (2020) DNA and RNA cleavage complexes and repair pathway for TOP3B RNA- and DNA-protein crosslinks. *Cell Rep.*, **33**, 108569.
- Stoll, G., Pietilainen, O.P.H., Linder, B., Suvisaari, J., Brosi, C., Hennah, W., Leppä, V., Tornaiainen, M., Ripatti, S., Ala-Mello, S. *et al.* (2013) Deletion of TOP3beta, a component of FMRP-containing mRNPs, contributes to neurodevelopmental disorders. *Nat. Neurosci.*, **16**, 1228–1237.
- Yang, X., Saha, S., Yang, W., Neuman, K.C. and Pommier, Y. (2022) Structural and biochemical basis for DNA and RNA catalysis by human topoisomerase 3beta. *Nat. Commun.*, **13**, 4656.
- Lee, S.K., Xue, Y., Shen, W., Zhang, Y., Joo, Y., Ahmad, M., Chinen, M., Ding, Y., Ku, W.L., De, S. *et al.* (2018) Topoisomerase 3beta interacts with rna1 machinery to promote heterochromatin formation and transcriptional silencing in Drosophila. *Nat. Commun.*, **9**, 4946.
- Sims, R.J. 3rd, Rojas, L.A., Beck, D.B., Bonasio, R., Schuller, R., Drury, W.J. 3rd, Eick, D. and Reinberg, D. (2011) The C-terminal domain of RNA polymerase II is modified by site-specific methylation. *Science*, **332**, 99–103.
- Yang, Y., Lu, Y., Espejo, A., Wu, J., Xu, W., Liang, S. and Bedford, M.T. (2010) TDRD3 is an effector molecule for arginine-methylated histone marks. *Mol. Cell*, **40**, 1016–1023.
- Kashima, I., Jonas, S., Jayachandran, U., Buchwald, G., Conti, E., Lupas, A.N. and Izaurralde, E. (2010) SMG6 interacts with the exon junction complex via two conserved EJC-binding motifs (EBMs) required for nonsense-mediated mRNA decay. *Genes Dev.*, **24**, 2440–2450.
- Dikic, I. and Elazar, Z. (2018) Mechanism and medical implications of mammalian autophagy. *Nat. Rev. Mol. Cell Biol.*, **19**, 349–364.
- Scott, R.C., Schuldiner, O. and Neufeld, T.P. (2004) Role and regulation of starvation-induced autophagy in the Drosophila fat body. *Dev. Cell*, **7**, 167–178.
- Peeters, J.G.C., Picavet, L.W., Coenen, S., Mauthe, M., Vervoort, S.J., Mocholi, E., de Heus, C., Klumperman, J., Vastert, S.J., Reggiori, F. *et al.* (2019) Transcriptional and epigenetic profiling of nutrient-deprived cells to identify novel regulators of autophagy. *Autophagy*, **15**, 98–112.
- Kwan, K.Y. and Wang, J.C. (2001) Mice lacking DNA topoisomerase β develop to maturity but show a reduced mean lifespan. *Proc. Natl. Acad. Sci. U.S.A.*, **98**, 5717–5721.
- Rubinsztein, D.C., Marino, G. and Kroemer, G. (2011) Autophagy and aging. *Cell*, **146**, 682–695.
- Kim, D., Paggi, J.M., Park, C., Bennett, C. and Salzberg, S.L. (2019) Graph-based genome alignment and genotyping with HISAT2 and HISAT-genotype. *Nat. Biotechnol.*, **37**, 907–915.
- Anders, S., Pyl, P.T. and Huber, W. (2015) HTSeq—a Python framework to work with high-throughput sequencing data. *Bioinformatics*, **31**, 166–169.
- Love, M.I., Huber, W. and Anders, S. (2014) Moderated estimation of fold change and dispersion for RNA-seq data with DESeq2. *Genome Biol.*, **15**, 550.
- Langmead, B., Trapnell, C., Pop, M. and Salzberg, S.L. (2009) Ultrafast and memory-efficient alignment of short DNA sequences to the human genome. *Genome Biol.*, **10**, R25.
- 1000 Genome Project Data Processing Subgroup, Li, H., Handsaker, B., Wysoker, A., Fennell, T., Ruan, J., Homer, N., Marth, G., Abecasis, G. and Durbin, R. (2009) The sequence alignment/map format and samtools. *Bioinformatics*, **25**, 2078–2079.
- Ramirez, F., Dundar, F., Diehl, S., Gruning, B.A. and Manke, T. (2014) deepTools: a flexible platform for exploring deep-sequencing data. *Nucleic Acids Res.*, **42**, W187–W191.
- Quinlan, A.R. and Hall, I.M. (2010) BEDTools: a flexible suite of utilities for comparing genomic features. *Bioinformatics*, **26**, 841–842.
- Zhang, Y., Liu, T., Meyer, C.A., Eeckhoutte, J., Johnson, D.S., Bernstein, B.E., Nusbaum, C., Myers, R.M., Brown, M., Li, W. *et al.* (2008) Model-based analysis of ChIP-Seq (MACS). *Genome Biol.*, **9**, R137.
- Heinz, S., Benner, C., Spann, N., Bertolino, E., Lin, Y.C., Laslo, P., Cheng, J.X., Murre, C., Singh, H. and Glass, C.K. (2010) Simple combinations of lineage-determining transcription factors prime cis-regulatory elements required for macrophage and B cell identities. *Mol. Cell*, **38**, 576–589.
- Parua, P.K., Kalan, S., Benjamin, B., Sanso, M. and Fisher, R.P. (2020) Distinct Cdk9-phosphatase switches act at the beginning and end of elongation by RNA polymerase II. *Nat. Commun.*, **11**, 4338.
- Teytelman, L., Thurtle, D.M., Rine, J. and van Oudenaarden, A. (2013) Highly expressed loci are vulnerable to misleading ChIP localization of multiple unrelated proteins. *Proc. Natl. Acad. Sci. U.S.A.*, **110**, 18602–18607.
- Wang, J.D., Cao, Y.L., Li, Q., Yang, Y.P., Jin, M., Chen, D., Wang, F., Wang, G.H., Qin, Z.H., Hu, L.F. *et al.* (2015) A pivotal role of FOS-mediated BECN1/Beclin 1 upregulation in dopamine D2 and D3 receptor agonist-induced autophagy activation. *Autophagy*, **11**, 2057–2073.
- Rusten, T.E., Lindmo, K., Juhasz, G., Sass, M., Seglen, P.O., Brech, A. and Stenmark, H. (2004) Programmed autophagy in the Drosophila fat body is induced by ecdysone through regulation of the PI3K pathway. *Dev. Cell*, **7**, 179–192.
- Bampton, E.T., Goemans, C.G., Niranjana, D., Mizushima, N. and Tolkovsky, A.M. (2005) The dynamics of autophagy visualized in live cells: from autophagosome formation to fusion with endo/lysosomes. *Autophagy*, **1**, 23–36.
- Merino, A., Madden, K.R., Lane, W.S., Champoux, J.J. and Reinberg, D. (1993) DNA topoisomerase I is involved in both repression and activation of transcription. *Nature*, **365**, 227–232.

38. Shykind, B.M., Kim, J., Stewart, L., Champoux, J.J. and Sharp, P.A. (1997) Topoisomerase I enhances TFIIID-TFIIA complex assembly during activation of transcription. *Genes Dev.*, **11**, 397–407.
39. Ahmad, M., Shen, W., Li, W., Xue, Y., Zou, S., Xu, D. and Wang, W. (2017) Topoisomerase 3beta is the major topoisomerase for mRNAs and linked to neurodevelopment and mental dysfunction. *Nucleic Acids Res.*, **45**, 2704–2713.
40. Zhao, D.Y., Gish, G., Braunschweig, U., Li, Y., Ni, Z., Schmitges, F.W., Zhong, G., Liu, K., Li, W., Moffat, J. *et al.* (2016) SMN and symmetric arginine dimethylation of RNA polymerase II C-terminal domain control termination. *Nature*, **529**, 48–53.
41. Kouzine, F., Gupta, A., Baranello, L., Wojtowicz, D., Ben-Aissa, K., Liu, J., Przytycka, T.M. and Levens, D. (2013) Transcription-dependent dynamic supercoiling is a short-range genomic force. *Nat. Struct. Mol. Biol.*, **20**, 396–403.
42. King, I.F., Yandava, C.N., Mabb, A.M., Hsiao, J.S., Huang, H.S., Pearson, B.L., Calabrese, J.M., Starmer, J., Parker, J.S., Magnuson, T. *et al.* (2013) Topoisomerases facilitate transcription of long genes linked to autism. *Nature*, **501**, 58–62.
43. Baranello, L., Wojtowicz, D., Cui, K., Devaiah, B.N., Chung, H.J., Chan-Salis, K.Y., Guha, R., Wilson, K., Zhang, X., Zhang, H. *et al.* (2016) RNA polymerase II regulates topoisomerase I activity to favor efficient transcription. *Cell*, **165**, 357–371.
44. Kwan, K.Y., Greenwald, R.J., Mohanty, S., Sharpe, A.H., Shaw, A.C. and Wang, J.C. (2007) Development of autoimmunity in mice lacking DNA topoisomerase 3beta. *Proc. Natl. Acad. Sci. U.S.A.*, **104**, 9242–9247.
45. Bunch, H., Lawney, B.P., Lin, Y.F., Asaithamby, A., Murshid, A., Wang, Y.E., Chen, B.P. and Calderwood, S.K. (2015) Transcriptional elongation requires DNA break-induced signalling. *Nat. Commun.*, **6**, 10191.
46. Camacho-Carranza, R., Membrillo-Hernandez, J., Ramirez-Santos, J., Castro-Dorantes, J., Chagoya de Sanchez, V. and Gomez-Eichelmann, M.C. (1995) Topoisomerase activity during the heat shock response in *Escherichia coli* K-12. *J. Bacteriol.*, **177**, 3619–3622.
47. Haffner, M.C., Aryee, M.J., Toubaji, A., Esopi, D.M., Albadine, R., Gurel, B., Isaacs, W.B., Bova, G.S., Liu, W., Xu, J. *et al.* (2010) Androgen-induced TOP2B-mediated double-strand breaks and prostate cancer gene rearrangements. *Nat. Genet.*, **42**, 668–675.
48. Mabb, A.M., Simon, J.M., King, I.F., Lee, H.M., An, L.K., Philpot, B.D. and Zylka, M.J. (2016) Topoisomerase I regulates gene expression in neurons through cleavage complex-dependent and -independent mechanisms. *PLoS One*, **11**, e0156439.
49. Puc, J., Kozbial, P., Li, W., Tan, Y., Liu, Z., Suter, T., Ohgi, K.A., Zhang, J., Aggarwal, A.K. and Rosenfeld, M.G. (2015) Ligand-dependent enhancer activation regulated by topoisomerase-I activity. *Cell*, **160**, 367–380.
50. Herrero-Ruiz, A., Martinez-Garcia, P.M., Terron-Bautista, J., Millan-Zambrano, G., Lieberman, J.A., Jimeno-Gonzalez, S. and Cortes-Ledesma, F. (2021) Topoisomerase IIalpha represses transcription by enforcing promoter-proximal pausing. *Cell Rep.*, **35**, 108977.
51. Khazeem, M.M., Casement, J.W., Schlossmacher, G., Kenneth, N.S., Sumbung, N.K., Chan, J.Y.T., McGow, J.F., Cowell, I.G. and Austin, C.A. (2022) TOP2B Is required to maintain the adrenergic neural phenotype and for ATRA-induced differentiation of SH-SY5Y neuroblastoma cells. *Mol. Neurobiol.*, **59**, 5987–6008.
52. McNamara, S., Wang, H., Hanna, N. and Miller, W.H. Jr (2008) Topoisomerase IIbeta negatively modulates retinoic acid receptor alpha function: a novel mechanism of retinoic acid resistance. *Mol. Cell Biol.*, **28**, 2066–2077.
53. Madabhushi, R., Gao, F., Pfenning, A.R., Pan, L., Yamakawa, S., Seo, J., Rueda, R., Phan, T.X., Yamakawa, H., Pao, P.C. *et al.* (2015) Activity-induced DNA breaks govern the expression of neuronal early-response genes. *Cell*, **161**, 1592–1605.
54. Di Malta, C., Cinque, L. and Settembre, C. (2019) Transcriptional regulation of autophagy: mechanisms and diseases. *Front. Cell Dev. Biol.*, **7**, 114.